PHYSICAL REVIEW C VOLUME 17, NUMBER 2 FEBRUARY 1978

Surface transparent potentials and a coupled-channel Born-approximation study of diffractive behavior in heavy-ion induced reactions*

A. J. Baltz and S. Kahana
Brookhaven National Laboratory, Upton, New York 11973
(Received 7 September 1977)

Coupled channel explanations, which have been offered for the diffractive behavior observed in the differential ground state-ground state cross sections of (^{16}O,^{18}O) reactions on Ni isotopes, are in apparent disagreement with data for transfer to the ^{18}O(2$^+$) state. A study of available quasielastic reaction data, elastic, inelastic, and transfer suggests the surface-transparent potentials both can better describe the optical phenomena observed in the angular shapes and can minimize effects due to coupled channels. As a by-product a description, which does not require a large ^{18}O(2_1^+) quadrupole moment, is obtained for the troublesome angular distribution in ^{18}O + ^{58}Ni inelastic scattering.

[NUCLEAR REACTIONS CCBA analysis (^{16}O, ^{18}O) reaction on Ni isotopes and all related quasielastic processes. Dependence on optical potentials examined.]

I. INTRODUCTION

In several studies[1-3] of specific heavy-ion induced one and two particle transfer reactions it was noted that adequate fits to data could be obtained only if surface transparent potentials were employed, at least within the context of the distorted-wave–Born-approximation (DWBA). More recently[4] an interesting reanalysis of the reaction

$$^{60}\mathrm{Ni}(^{18}\mathrm{O},^{16}\mathrm{O})^{62}\mathrm{Ni} \qquad (1)$$

including coupling to the excited ^{18}O(2$^+$) channel, attempted to reinstate the more conventional "strong absorption" potentials. The phenomenon under specific consideration is the forward rising oscillatory pattern often evident above certain bombarding energies in the angular distributions of the transfer reactions.[1,2,5] The earlier work[1,2] views these diffractive angular distributions as the result of interference between a peripheral Coulomb-dominated projectile-orbit on one side of the target nucleus and a slightly penetrating orbit on the far side. Thus too strong an absorption in the nuclear surface would severely reduce the penetrating flux and extinguish the interference pattern. The reanalysis does not question the optical nature of the phenomenon, but instead of enhancing the contribution from the penetrating orbit by choice of optical potential, diminishes that from the peripheral orbit by cancellation between one and two step transfer routes. Clearly this is an issue of some importance perhaps easily settled since it is raised in such an unambiguous fashion. It is our intention to show the inclusion of higher order corrections to DWBA strengthens, rather than weakens, the case for surface transparency.

An interesting by-product of our investigation concerns the inelastic excitation of the projectile ^{18}O in ^{58}Ni+^{18}O. Several investigations[6,7] have noted difficulties in fitting the prominent Coulomb-nuclear interference dip observed in the angular distribution for inelastic excitation of ^{18}O(2_1^+). Remedies have been proposed for treating this difficulty; one of which[6] requires reorientation through an extraordinarily large ^{18}O(2_1^+) quadrupole moment. We find yet another prescription, which, however, should follow from microscopic or semimicroscopic evaluations of the inelastic form factor. Within our calculations the effect of reorientation is small.

Ultimately it is a confrontation of these phenomenological models with the quasielastic (transfer, elastic, and inelastic) data that will prove decisive; a first principles calculation of the absorptive potential is not yet at hand. Of vital importance is the reaction

$$^{60}\mathrm{Ni}(^{16}\mathrm{O},^{18}\mathrm{O}(2_1^+))^{58}\mathrm{Ni}, \qquad (2)$$

noted, but perhaps not sufficiently heeded in Ref. 4. The observed strength of reaction (2) provided a basis of including channel coupling in the theory for the ground-state–ground-state (g.s.-g.s.) reaction (1). It is logical that the (^{16}O, ^{18}O(2$^+$)) transfer data be explained by a scheme using such projectile excitation as a vital indirect route in the ground-state transfer. In fact the predictions of the strongly absorbing model are in clear disagreement with this data.[8] The observed ^{18}O(2$^+$) excitation exhibits a differential cross section, flat at intermediate angles and rising sharply toward the most forward angles, whereas the distribution predicted from strong absorption and pro-

jectile excitation is bell-shaped,[4] peaking near 40° in the center of mass. The observed angular shape for transfer to the $^{18}O(2^+)$ state is reminiscent of the envelope of that to the ground state, suggesting a common explanation. Further, we note the ratio of excited projectile to ground-state routes was almost certainly overestimated in the strong absorption calculation. This ratio was taken[4] from the observed value of 3.4 at $\theta_{c.m.} = 32.6°$ while the overall average at measured angles is nearer 2 (see Figs. 1 and 2).

The role played by the shape of the angular distribution in reactions (1) and (2) can be better understood if one examines the philosophy of multistep, or more specifically, coupled-channel, approaches to direct reactions. The distorted-wave Born approximation can be thought of as the first perturbative term in a multistep calculation. The size and character of this first term, and presumably also of the remaining terms in the series, depend to some extent on the choice of optical potential. It seems apparent that the optical potential should be taken to minimize, rather than maximize, corrections beyond the Born approximation. Further, it is reasonable to incorporate into the optical potential any effect common to several target or projectile excited states, i.e., to several of the coupled channels. Since both ground and excited 2_1^+ state in the (^{16}O, ^{18}O) reactions are observed to rise towards forward angles it seems unnatural to begin with direct angular distributions which fall for small $\theta_{c.m.}$, and to achieve the observed, differential cross sections from higher order processes. Even should the introduction of yet higher excited states, for example the 4_1^+ in addition to the 2_1^+ state of ^{18}O, prove quantitatively necessary, the data suggest that the oscillatory, forward-peaked distribution is an optical phenomenon properly described in an average way by the optical potential. In practice we demonstrate that the inclusion of at least the next group of ^{18}O excited states does not save the situation for the strongly absorbing potentials.

Although the surface transparent and strongly absorbing potentials can yield similar angular shapes for the ground-state–ground-state transition they lead to *quite different* absolute magnitudes. In fact, it is somewhat paradoxical that the calculation beginning with strong absorption ends up *after* channel coupling, which presumably generates even more absorption, with an angular distribution that can be attributed to surface penetration. This sleight of hand is accomplished not by appreciably increasing the amount of penetrating flux but rather by a rather drastic reduction in the peripheral or Coulomb-dominated flux. The overall effect is to greatly reduce cross-section magnitudes, not necessarily a situation to be favored since theoretical calculations for two nucleon transfer already notoriously underpredict observed magnitudes.

A final point to be made about the calculation in Ref. 4 is of a more minor nature. The predicted oscillations at angles between $\theta_{c.m.} = 15°$ and 25° are out of phase with the Brookhaven data.[4] This result follows to some extent from the use of a real optical potential fitted to elastic scattering in $^{18}O + ^{58}Ni$ rather than in $^{18}O + ^{60}Ni$. In an earlier paper discussing the isotopes $^{58,60,62,64}Ni$ quite substantial deviation from an $(A_1^{1/3} + A_2^{1/3})$ mass dependence were noted in potential parameters. However, in the present work we will try to avoid such deviations, selecting ^{16}O, ^{18}O potentials which apparently work well for several of the Ni isotopes, i.e., fit available scattering data.

Our approach, in what follows, will be to perform two parallel calculations, one with the strong absorbing potential of Ref. 4 and another with the surface transparent potential similar to that in Refs. 2 and 3. These calculations include coupling not only to the first excited states of ^{18}O but also to the 4_1^+, 2_2^+, and 0_2^+ states, the latter states playing only a minimal role. With respect to an ^{18}O initiated reaction we consider the ^{58}Ni as well as ^{60}Ni targets. The transfer cross sections were calculated using slightly modified versions of the finite-range codes SATURN and MARS[9] of Tamura, Udagawa, and Low. The inelastic and elastic cross sections were obtained with the coupled-channel code CHUCK of Kunz.[10]

II. DISTORTED-WAVE BORN-APPROXIMATION DESCRIPTION OF THE REACTIONS

It is well to review the predictions for the two inverse reactions Eq. (1) and Eq. (2) obtained from a purely distorted-wave one step approach (DWBA). In the earliest presentation[1] forward rising cross sections were observed for the $^{58,60}Ni(^{18}O, ^{16}O)$-$^{60,62}Ni$(g.s.) reactions at 65 MeV and subsequently oscillations were predicted in calculations employing optical potentials which weakened the absorption not only in the region of surface penetration but also at deeper penetration. In ensuing work[2,3] strong oscillations were observed in $^{60}Ni(^{18}O, ^{16}O)$-^{62}Ni(g.s.) and a vastly superior theoretical description obtained with a surface-transparent volume-opaque absorption. The potential used in Ref. 2 is reintroduced as *P*1 in Table I and the resulting theoretical ground state and ^{18}O (2^+) angular distributions displayed in Figs. 1 and 2. A diffusivity of 0.05–0.30 may be used for the volume absorptive potential without substantially changing the re-

TABLE I. Optical potentials used in the various elastic, inelastic, and transfer calculations. $P2$ is representative of the so-called strong absorbing potentials, possessing a deeper imaginary part which also extends furthest outwards from the region of nuclear interaction. $P1$ is an early (Ref. 2) version of the surface transparent-volume opaque potentials, $P3$, $P4$, $P5$ are also in this family but designed to be used in the CCBA calculations in the present work. $P2$ consists of potentials for both ^{16}O+ Ni and ^{18}O+ Ni channels. The potentials $P3$, $P4$ for ^{18}O, ^{16}O, respectively, were employed with a varying but small value for the surface absorption depth W_S. The volume real potential is a standard Woods-Saxon potential, the imaginary potential is as given in Eqs. (13) to (17) in the text. All radius parameters are interpreted as

$$R = r_0(A^{1/3}_{\text{projectile}} + A^{1/3}_{\text{target}}) .$$

Potential		V_R	W_V (MeV)	W_S	r_{0R}	r_{0V}	r_{0S} (fm)	r_{0C}	a_R	a_V	a_S
$P1$	^{18}O	70	18	1	1.328	1.282	1.378	1.328	0.40	0.05	0.40
	^{16}O	70	18	1	1.283	1.237	1.283	1.283	0.40	0.05	0.40
$P2$	^{18}O	70	45	0	1.19	1.19	···	0.73	0.56	0.56	···
	^{16}O	70	18	0	1.19	1.19	···	1.19	0.54	0.54	···
$P3$	^{18}O	70	18	0–3.5	1.292	1.20	1.20	1.292	0.45	0.20	0.45
$P4$	^{16}O	70	18	0–3.5	1.205	1.20	1.20	1.299	0.51	0.25	0.45
$P5$	^{16}O	70	18	0–3.5	1.24	1.20	1.20	1.299	0.45	0.25	0.45
$P6$	^{16}O	70	18	0–3.5	1.2	1.2	1.2	1.299	0.45	0.25	0.45

sults; the larger values seem more reasonable. The distorted-wave code used to obtain the results of Fig. 1 was **DRC II**, a no-recoil code[11] incorporating a microscopic two nucleon form factor. A scaling parameter present in the code was adjusted to simulate the effects of recoil. An expansion about the no recoil approximation, directed towards achieving the exact finite range result, has been discussed[12,13] and shown to remove the α de-

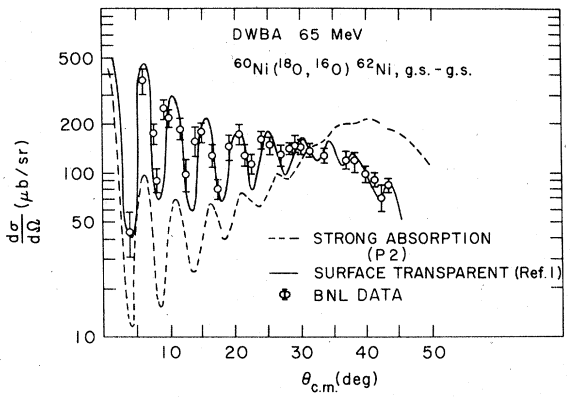

FIG. 1. Comparison between DWBA and experiment for $^{60}Ni(^{18}O, ^{16}O)^{62}Ni$(g.s.) at 65 MeV. The strong absorption calculation made in the cluster approximation discussed in Sec. IV, and using $P2$ (Table I), closely approximates that of Ref. 4. The surface transparent calculation is taken from Ref. 2, and involves a microscopic no-recoil form factor with $P1$ (Table I). Normalization is at this point arbitrary.

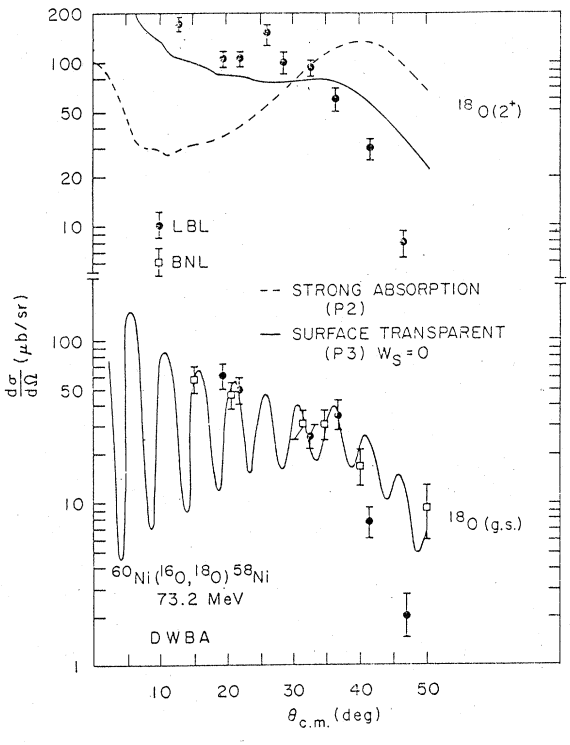

FIG. 2. DWBA for $^{60}Ni(^{16}O, ^{18}O)^{58}Ni$ at 73.2 MeV [equivalent to 65 MeV $(^{18}O, ^{16}O)$]. Theoretical cluster calculations are made for the following: (1) the strong absorbing potential $P2$ for ^{16}O and ^{18}O, (2) the surface transparent potentials $P3$ (^{18}O), $P4$ (^{16}O) from Table I. The strong absorption shape for the ^{18}O g.s. is similar to that shown in Fig. 1. Normalizations are again arbitrary.

pendence for single-nucleon transfer. The shape of differential cross section obtained in DWBA is dependent to some extent on α, but sufficient freedom exists in fitting the elastic data to permit the α dependence in DWBA to be compenstated for by the choice of potential parameters. Since in any case we believe recoil effects are *crucial* once channels other than elastic are included, it is pointless to overemphasize the particular choice of no-recoil approximation used previously.

The strong absorption potential used in Ref. 4 is also given in Table I, as $P2$, and the two neutron ground-state–ground-state differential cross section from this potential is displayed in Fig. 1. The single step DWBA using $P2$ is obtained in a full recoil but cluster approximation described in the next section. The angular distribution obtained in this manner is similar but not identical to that found in a microscopic recoil or no-recoil DWBA calculation.[4] The data indicated by open circles in Fig. 1 are from Ref. 2 and were taken at the Brookhaven National Laboratory tandem with the quadrupole-dipole-dipole-dipole magnetic spectrometer. Data also exist for the reaction ^{60}Ni(^{16}O, ^{18}O)^{58}Ni at 73.2 MeV, i.e., for the inverse pickup reaction in Eq. (2). These latter data from the Lawrence Berkeley Laboratory 88-inch cyclotron, as yet unpublished,[8] are also displayed in Fig. 2 for transitions to the ^{18}O ground and first excited (2^+) states. The LBL ground-state data agree very well with the Brookhaven data except perhaps at the most backward angles measured. The DWBA predictions from two standard potentials employed further in this work in Table I, $P2$ (strong absorbing), $P3$ (surface transparent), are also compared with the data for transition to the 2^+ state of ^{18}O. An altered surface transparent potential $P3$ is employed for the A-2 targets consistent with the demands of elastic data. This point will be discussed in greater detail later where a consistent single set of potential parameters is generated capable of describing reactions on the several Ni isotopes considered here. In both Fig. 1 and Fig. 2, for the moment, arbitrary normalizations of the theoretical curves are used. Also, when we have reconstructed weak and strong absorption calculations within a single model, magnitudes will be compared. For the present we note that $P1$ in Table I underpredicts the observed ground-state–ground-state cross section by a factor of approximately 4. The microscopic form factor used in this calculation is discussed in Refs. 11 and 5 and uses relatively simple (sd)-shell and (pf)-shell wave functions for ^{18}O and ^{60,62}Ni.

Clearly if one were to stop with the DWBA calculations, the surface transparent potentials would be preferred. Whether or not this situation persists as one includes coupling to strong inelastic channels remains to be seen. A quite drastic interference phenomenon must result from second order processes if the angular distributions from the strongly absorbing potentials are to explain the data for both ground state *and* excited states.

It is well to note at this point the single step distorted-wave calculations provide us with an operational definition of surface transparency. It is fairly evident from Table I that $P1$ and $P3$ possess considerably weaker imaginary parts than does $P2$ for larger ion-ion separations, i.e., in the nuclear interaction "surface." However, an actual measure of how absorptive a potential is depends also on the real part of the potential. For present purposes then a strongly absorbing potential is one, like $P2$, which predicts smooth bell-shaped angular distributions for the g.s.-g.s. ^{58,60}Ni(^{18}O, ^{16}O) reactions at the energies considered here, i.e., in the neighborhood of 60–65 MeV or approximately at twice the Coulomb barrier. Clearly at sufficiently low energies where Coulomb forces keep target and projectile well apart all transfer cross sections acquire this standard shape. In Secs. III and IV we discuss the dependence of our predictions on two vital parameters, the diffusivity a_I of the voume absorption and the depth W_S of the surface absorption.

It will be our general contention that the ^{60}Ni-(^{16}O, ^{18}O(2^+))^{58}Ni angular distribution can be described in a theory including coupling to a small number of low lying projectile (or target) states only if the ^{18}O(g.s.) distribution is already well described in DWBA.

III. OPTICAL POTENTIALS, ELASTIC SCATTERING, AND INELASTIC EXCITATION

It is traditional in a distorted-wave analysis to imagine that the optical potentials may be deduced unambiguously from analysis of elastic scattering. Unfortunately presently measured heavy-ion elastic data, at least for angles where the differential elastic cross section remains larger than say 1% of Rutherford, is relatively insensitive to the component of the optical potential of particular interest here, i.e., the absorption. This observation does not preclude the possibility that some optical data are relevant to the present issue. Recent data from Brookhaven National Laboratory on ^{16}O + ^{28}Si at 55 and 60 MeV (Ref. 14) seem to support the choice of surface transparent potentials; the elastic to Coulomb ratio is seen to halt its downward plunge, levels off at about 10^{-3}, exhibits rather narrow oscillations in angle, and further rises dramatically at back angles. This

very interesting elastic data and the related question of the validity of a spherical optical potential description of the backward angle data will not be pursued in this work. One feature of the differential elastic cross section which appears responsive to changes in the degree of absorption is the magnitude of the Fresnel oscillations at angles forward of the grazing angle, in particular the height of the Coulomb rainbow peak. However, these magnitudes also depend on other optical parameters, and to draw any conclusions one would have to take very seriously the degree of confidence established statistically in elastic searches.

We have pointed out in the past[1,5] that the transfer differential cross-section shapes are very sensitive to the absorption. In fact, the transfer reactions, elastic and inelastic scattering, i.e., all quasielastic reactions, should not be treated separately. A coherent picture of all these reactions must be achieved by any viable reaction theory. Such a statement is certainly self-evident when the reaction theory includes channel coupling. A minimum set of data to examine in beginning a model calculation consists of elastic scattering together with inelastic excitations to any low lying excited states of the projectile or target. If the inelastic excitations were treated microscopically then an additional element to be specified in the theory would be a two body residual interaction, in principle calculable from first principles. In a completely macroscopic description[15] the operator effecting the inelastic excitation is in form derivable from the optical potential and in magnitude partly determined by electromagnetic transition data. An intermediate semimicroscopic situation, very like that obtaining for transfer, occurs if a single folding is done of the microscopic form factor.

In a distorted-wave treatment of the reaction

$$A_i + B \to A_f + B \tag{3}$$

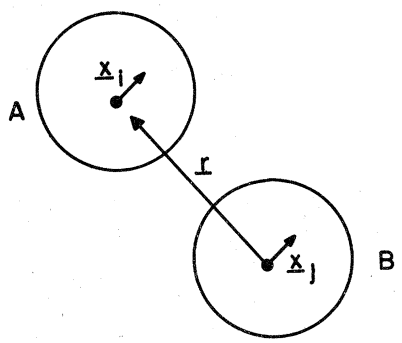

FIG. 3. Coordinates for inelastic excitation of ^{18}O and ^{58}Ni during scattering.

the transition amplitude may be written[15]

$$M = \int d^3\vec{r}\,\chi_f^{*(-)}(\vec{r})(\Phi^f_{A,B}|(V-U)|\Phi^i_{A,B})\chi_i^{(+)}(\vec{r}). \tag{4}$$

In Eq. (4) the optical potential is

$$U = U(\vec{r}), \tag{5}$$

while for a microscopic approach the interaction producing the transition is

$$V = \sum_{\substack{i\in A\\ j\in B}} v_{ij}(\vec{x}_i - \vec{x}_j + \vec{r}) \tag{6}$$

with the coordinates as indicated in Fig. 3. The form factor

$$F(\vec{r}) = (\Phi^f_{A,B}|(V-U)|\Phi^i_{A,B}) \tag{7}$$

may be evaluated in each of the several manners described above. The semimicroscopic treatment would, for example, integrate Eq. (7) over the coordinates $\vec{x}_j$ of the unexcited nucleus B, yielding

$$(\Phi_B|V|\Phi_B) = \sum_{i,\beta}\int d_3x\,\varphi^*_\beta(\vec{x})\varphi_\beta(\vec{x})v(\vec{x}-\vec{x}_i+\vec{r})$$

$$= \sum_i V_{\text{eff}}(\vec{r}-\vec{x}_i). \tag{8}$$

The interaction V_{eff} obtained in this fashion closely resembles that used in transfer and may be regarded as a summation over the shell model potentials felt by the A nucleons in the presence of B. If the inelastic transition $A_i \to A_f$ involves, say, nucleons in a limited number of external levels $[a,a']$, the resultant form factor will appear as

$$F(\vec{r}) = (\Phi^f_A|V_{\text{eff}}|\Phi^i_A)$$

$$= \sum_{aa'} c_{aa'}\int d^3\vec{x}_i\,\phi^*_a(\vec{x}_i)V_{\text{eff}}(\vec{r}-\vec{x}_i)\phi_{a'}(\vec{x}_i). \tag{9}$$

If the bound state wave functions $\phi_a(\vec{x}_i)$ fall off more slowly for $x_i \to \infty$ than V_{eff} one then expects as $r \to \infty$

$$F(\vec{r}) \sim (\phi^*_a\phi_{a'}) \sim [\phi_a(r)\phi_{a'}(r)]_{\text{radial}}. \tag{10}$$

A macroscopic approach identifies $(\Phi^f_{A,B}|V|\Phi^i_{A,B})$ with a vibrational or deformed optical potential and the form factor is[15]

$$F(\vec{r}) = U\left[r\left(1 - \sum_{\lambda\mu}\alpha^\lambda_\mu Y^\lambda_\mu\right)\right] - U(r). \tag{11}$$

For example, small amplitude excitation of a (2^+) state in either a rotational or vibrational nucleus would use

$$F(\vec{r},\beta) \approx +\beta\sum_\mu \frac{\partial U}{\partial r}(r)R_A((a^2_\mu)^\dagger Y^2_\mu + \text{H.c.}) \tag{12}$$

with β describing the extent of deformation and hence the strength of the excitation, while $(a^2_\mu)^\dagger$

creates a (2μ) phonon excitation in the nucleus A. $F(\vec{r})$ in Eq. (11) can, of course, also include excitation of B and the use of the radius R_A in Eq. (12) accounts for proper scaling of the excitation of A. The strength of the Coulomb piece of (12) can in the usual fashion[15] be related to the $[BE(\lambda)]^{1/2}$ transition amplitude for $(a \to a')$ in A.

In the context of the present problem it is likely excitations of ^{18}O which are perhaps not strongly collective are described by Eqs. (9) and (10) with those of ^{58,60}Ni better described by (11) and (12). For ^{18}O $(0_1^+ \to 2_1^+)$ one might then from (1) expect an effective form factor "diffusivity" to be $\gtrsim 1$ fm rather than about 0.5 fm. We believe from what follows that either the complete or semimicroscopic descriptions are necessary if full justice is to be done to the reaction theory, at least when treating light-heavy-ion projectile excitation. Difficulties exist in the distorted-wave treatments of the inelastic angular distributions with or without channel coupling, which have been noted by groups at the Niels Bohr Institute, RISO,[6] and at Munich.[7] The nature of the problem is displayed in Fig. 5 where data from RISO on the 60 MeV reaction ^{58}Ni(^{18}O, ^{18}O(2$^+$))^{58}Ni is compared with a DWBA calculation: The prominent Coulomb-nuclear interference dip in the angular distribution is shifted backward in the theory by about 4° in the center of mass. Similar problems do not seem to occur for target excitation. Various remedies have been presented for this failing. One has been to incorporate reorientation in a channel-coupling calculation, with what seems an abnormally large quadrupole moment[6,16] for the ^{18}O(2$^+$) state. A second has been to rotate the phase of the macroscopic form factor, obtained by differentiation of the optical potential; in fact to use a purely imaginary form factor.[7,17] The second of these approaches was adopted in Ref. 4 and we employ this technique to produce one of our parallel calculations (Fig. 4). A third approach we have followed is to attempt to simulate the effects of a microscopic calculation within the macroscopic framework. The ^{18}O valence nucleons which are probably principally involved in a more single-particle than collective excitation are rather loosely bound, and their slow fall off in space may be represented by adding to the form factor a component with a large diffusivity. This procedure which apparently was also discussed by Rother[18] will be shown to have a considerable degree of success, and is followed in our second and principal calculation of the reactions Eqs. (1) and (2). We increase the imaginary diffusivity also, although as usual this is harder to justify.

In any case, one may view the inelastic data as in extension of the elastic data, one more element to be used in constraining the details of the coupled-channel transfer calculation. The excitation of the low lying Ni(2_1^+) state is not negligible; the influence on angular distributions and cross-section magnitudes will be referred to separately, later. The projectile inelastic and elastic data are now described in coupled-channel calculations employing the coupled-channel program CHUCK of Kunz,[10] with ^{18}O(2_1^+) and then the 4_1^+, 0_2^+, and 2_2^+ excitations. These states are treated macroscopically with representative β values and βR values shown in Table II. Only β_2 values, i.e., corresponding to E_2 transitions, are used. The Coulomb piece of the macroscopic form factor for excitation of a given state is constrained by observed electromagnetic transitions, but in principle the magnitude of the nuclear component is undetermined. In practice one would like to use this freedom to fit the angular shape and magnitude of the inelastic differential cross sections. Only small differences seem necessary between $(\beta R)_{\text{Coulomb}}$ and $(\beta R)_{\text{nuclear}}$.

We now present the result of these coupled-channel investigations of the ^{18}O+^{58}Ni inelastic and elastic data at 50, 60, and 63 MeV and of ^{18}O+^{60}Ni data at 63 MeV. The calculations have been performed with CHUCK using the same number of partial waves (80) and cutoff radius (20 fm) as later employed in transfer. Necessarily our treatment of the Coulomb excitation is approximate, not accurate for angles further forward than those presented here in Figs. 4 to 11. At the angles considered comparison with more accurate (but less flexible) treatments of the Coulomb terms indicate only small errors of approximately a few percent. We have as stated included coupling to the 2_1^+ as well as to $4_1^+, 2_2^+, 0_2^+$ states of ^{18}O, but only the first excited state seems important in any of our models. Indeed as our results indicate the DWBA would give an excellent description of the process, for the optical potentials and form factors we favor, i.e., for the so-called surface transparent family of potentials. We have selected the N.B.I. 60 MeV ^{16}O+^{58}Ni data as a standard, i.e., for a determination of optical parameters. Elastic and inelastic data at other energies and on other Ni isotopes are predicted; no energy or nuclide variation (other than $A_O^{1/3}+A_{Ni}^{1/3}$) is permitted.

The higher states of ^{18}O seem to have little effect on the theoretical predictions, thus the comparison with data shown in Figs. 4 and 5 including only 2_1^+ coupling represent well the results of inelastic searches. In Fig. 4 the elastic and inelastic data at 60 MeV are compared with a reproduction of the calculation in Ref. 4. The optical potential in this latter calculation is $P2$ of Table I and the form factor parameters $F1$ are those in Table III, obtained from $P2$ by rotating the phase

TABLE II. Coupling strengths β_C (Coulomb) and β_N (nuclear) for coupled-channel inelastic and transfer. The $BE(2)$ values from which the β_C values are obtained are indicated as are effective nuclear strengths $(\beta R)_N$. The $0^+ \rightarrow 2^+$ coupling normalization is standard in all codes but the one- to two-phonon (e.g., $2_1^+ \rightarrow 4_1^+$, $0_1^+ \rightarrow 2_2^+$, etc.) normalization and reorientation sign $(2_1^+ \rightarrow 2_1^+)$ are not. In CHUCK the form factor radius R_C, and coupling β_C are defined by

$$\beta_C R_C^2 = \frac{4\pi}{3Z_{ex}} [BE(2)]^{1/2},$$

where Z_{ex} is the charge of the excited nucleus (projectile or target). In MARS the one- to two-phonon couplings β' are defined by $\beta_{CHUCK} = [2(2I+1)/5]^{1/2}\beta'$, I is the angular momentum of the 2 phonon state. Also in MARS the Coulomb coupling is correctly adjusted by a scaling of β' and compensatory rescaling of the nuclear form factor. In each of our calculations a common $\beta_C = \beta_N$ were used and the differences between nuclear and Coulomb adjusted by the above definitions in the codes.

Nucleus	Transition	Coulomb couplings $\beta_{II'}$ (CHUCK)	Nuclear βR (fm)	$BE(2)$ e^2 fm^4
^{18}O	$0_1^+ \rightarrow 2_1^+$	0.12(0.13)	1.01	40–48
	$2_1^+ \rightarrow 2_2^+$	0.12 → 0.24	1.01	
	$2_1^+ \rightarrow 4_1^+$	0.068 → 0.20	0.84	
	$2_1^+ \rightarrow 2_2^+$	0.17	1.43	
	$0_1^+ \rightarrow 2_2^+$	0.096	0.81	
^{58}Ni + ^{18}O	$0_1^+ \rightarrow 2_1^+$	0.112(0.103 MARS)	0.94	660
^{60}Ni + ^{16}O	$0_1^+ \rightarrow 2_1^+$	0.120(MARS)	0.93	930
^{62}Ni + ^{16}O	$0_1^+ \rightarrow 2_1^+$	0.117(MARS)	0.91	880
^{64}Ni + ^{16}O	$0_1^+ \rightarrow 2_1^+$	0.117(MARS)	0.92	880
^{66}Ni + ^{16}O	$0_1^+ \rightarrow 2_1^+$	0.117(MARS)	0.925	880

through 90° i.e., in place of the potential $U(r) = V_R + iW$ one uses $U(r) = i(V_R^2 + W^2)^{1/2}$. This rotation of phase has no apparent physical justification. The $(\beta R)_{nucleon}$ and $(\beta R)_{Coulomb}$ are 1.01 and 0.94 fm as in Ref. 4. In Fig. 5 the same comparison is made for the surface transparent $P3$ of Table I and with form factors $F2$ or $F3$ from Table III. In this case the form factor differs considerably from the usual macroscopic prescription, the real and imaginary diffusivities have been increased to a value $a_R = 1.12$ fm consistent with what is expected from the fall off for single valence particle wave functions in ^{18}O. Both approaches give a reasonably satisfactory description of the inelastic data, positioning the important nuclear-Coulomb dip correctly and yielding approximately correct

TABLE III. Inelastic form factors. Listed are the various form factors used in inelastic coupling in the form of potentials. Of course derivatives of these potentials are actually employed in the calculations. For the Ni excitations the form factors parameters are taken from the optical potentials in Table I. For ^{18}O excitation two approaches are used to fit the position of the nuclear-Coulomb dip: (1) rotation of the phase (2) increase in real and/or imaginary diffusivity. The latter we believe could follow from a semimicroscopic or microscopic treatment. The two form factors $F2$ and $F3$, which differ in their imaginary parts, yield identical results in excitation of ^{18}O(2_1^+); however, only $F2$ is used in the CCBA transfer calculations. The same form factors are used in $2_1^+ \rightarrow 4_1^+$ etc. as in $0_1^+ \rightarrow 2_1^+$.

		V_R	W_V (MeV)	W_S	r_{0R}	r_{0V}	r_{0S} (fm)	a_R	a_V	a_S
$F1$	^{18}O	···	70 × 1.849	···	1.19	1.19	···	0.56	0.56	
$F2$	^{18}O	50	18	4.5	1.131	1.131	1.131	1.12	0.20	1.12
$F3$	^{18}O	50	18	4.5	1.131	1.131	1.131	1.12	1.12	0.45

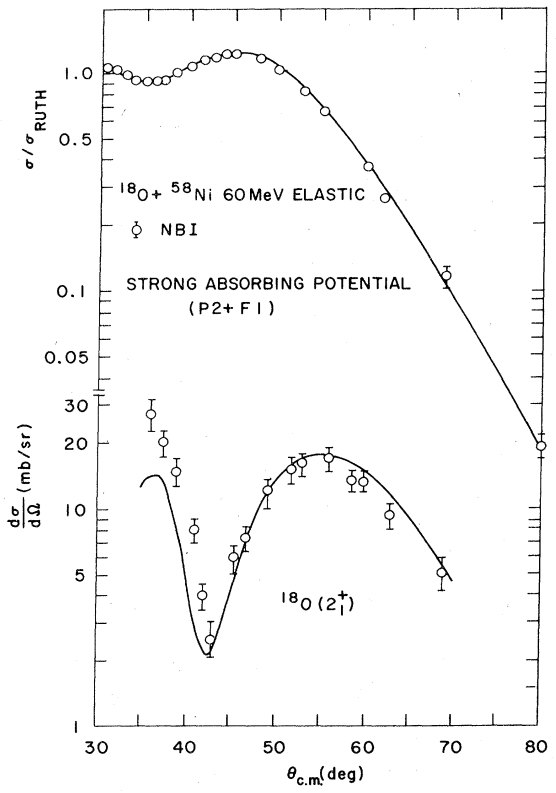

FIG. 4. Comparison between theory and experiment for $^{18}O+^{58}Ni$ elastic and inelastic 60 MeV scattering. Data are from the Niels Bohr Institute (Ref. 8). Theory is CCBA calculated in Ref. 4 and includes the 0_1^+ and 2_1^+ channels of ^{18}O. The coupling parameters are $(\beta R)_C = 0.94$ fm, $(\beta R)_N = 1.01$ fm while the elastic optical potential employed is $P2$ (^{18}O). The form factor is taken purely imaginary with $W_0' = (V_R^2 + W_0^2)^{1/2}$.

cross-section magnitudes. Elastic scattering is also very well described.

In Figs. 6 and 7 comparison is made between our standard calculation involving coupling to $^{18}O(2_1^+)$ and other obvious variations: DWBA coupled-channel including 0_1^+, 2_1^+, 4_1^+, or 0_1^+, 2_1^+, 2_2^+. The various coupling strengths $\beta_{0_1 2_2}, \beta_{2_1 2_2}, \beta_{2_1 4_1}$ appropriate to the code CHUCK were obtained from known electromagnetic transitions,[19] and these are summarized in Table II. Coupling to the 2_1^+ state is important only with use of the strongly absorbing potential and even here further coupling to the 4_1^+ seems insignificant. For the choice $P3$ and form factor $F2$, the single step DWBA works very well. Reorientation effects are shown in Fig. 7. For $|Q_0(2^+)| = |Q_{02}|$ (i.e., $\beta_{22} = \beta_{02} = 0.12$ in CHUCK) only a slight shift in the Coulomb-nuclear dip is seen. Even doubling this quadrupole moment changes the angular distribution only slightly. [The quadrupole moment for the $^{18}O(2_1^+)$ state is taken negative.]

Elastic and inelastic predictions for $^{18}O+^{58}Ni$ scattering at 50 and 63 MeV are compared with data for these energies in Fig. 8. A final point on $^{18}O+^{58}Ni$, 60 MeV scattering of considerable interest is contained in Fig. 7 where the inelastic cross section obtained when only the real form factor is given an extended tail is shown. Clearly interference between real and imaginary parts of the form factor is crucial in producing the rather deep dip observed experimentally. This real-imaginary interference plays a role in determining the importance of excited projectile state coupling in the transfer reactions. Predictions for $^{18}O+^{58}Ni$ data at 50 and 63 MeV are shown in Fig. 8.

We would like to have data on the pickup reaction for the ^{62}Ni target as well, i.e., on $^{16}O+^{62}Ni \rightarrow {}^{18}O(2^+)+{}^{60}Ni$. For completeness we present inelastic data and analysis for the $^{18}O+^{60}Ni$ target, using the identical potentials $P3$ from Table I and form factor $F2$ from Tables IV and V employed

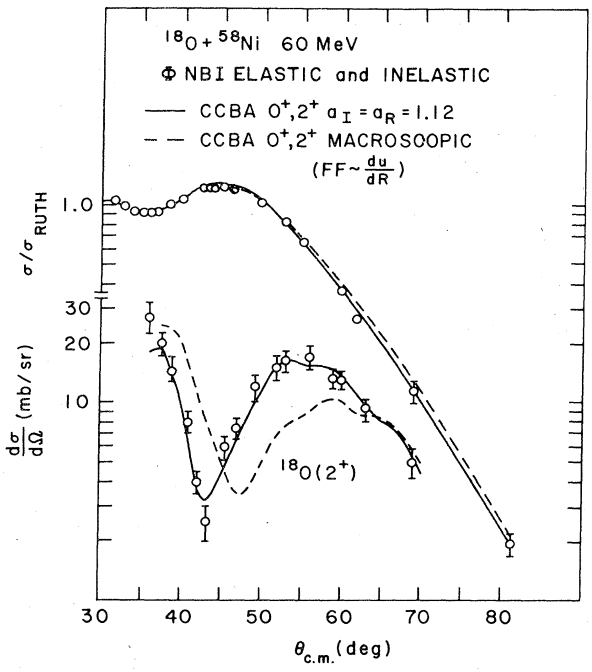

FIG. 5. Theory and experiment for $^{18}O+^{58}Ni$ at 60 MeV. Again CCBA (CHUCK) is with $^{18}O(0_1^+, 2_1^+)$ states but for the surface transparent potential $P3$ (Table I). The calculations were made with the form factor $F2$ as defined in Table III. Almost identical results obtain for $F3$ or if $W_S = 0$ in $P3$. Coupling parameters are as defined in Table II and yield $(\beta R)_N = 1.01$ fm and $\beta R_C{}^2 = 3.29$ fm^2. Shown are the results of using a purely macroscopic form factor and of a form factor extended to fall off like the bound valence neutrons in ^{18}O. The comparison with NBI data is used to determine a global potential which will predict other quasi-elastic reactions in the Ni isotopes.

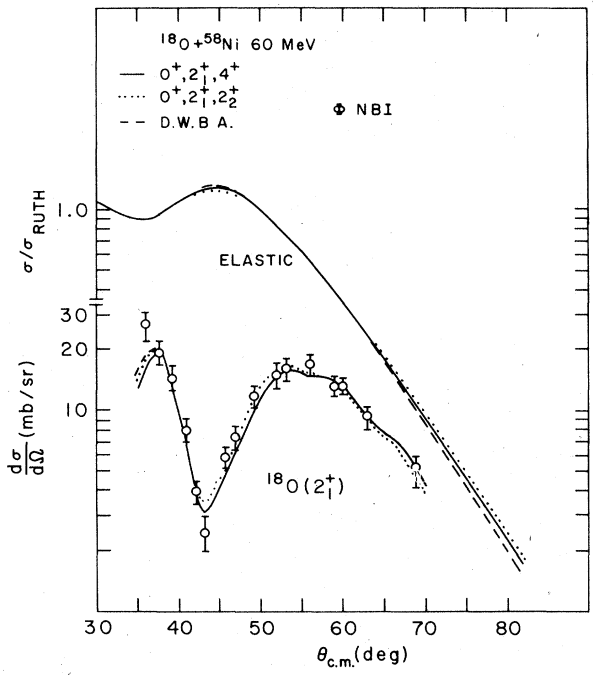

FIG. 6. Different CCBA couplings for the theory of Fig. 5. DWBA and the coupling 0_1^+, 2_1^+, 2_2^+ yield almost identical cross sections and only slightly different from that for 0_1^+, 2_1^+, 4_1^+. The coupling parameters are defined in Table II, the potential $P3$ from Table I. The potential parameters were not readjusted to yield identical elastic cross-sections, but differences are clearly small.

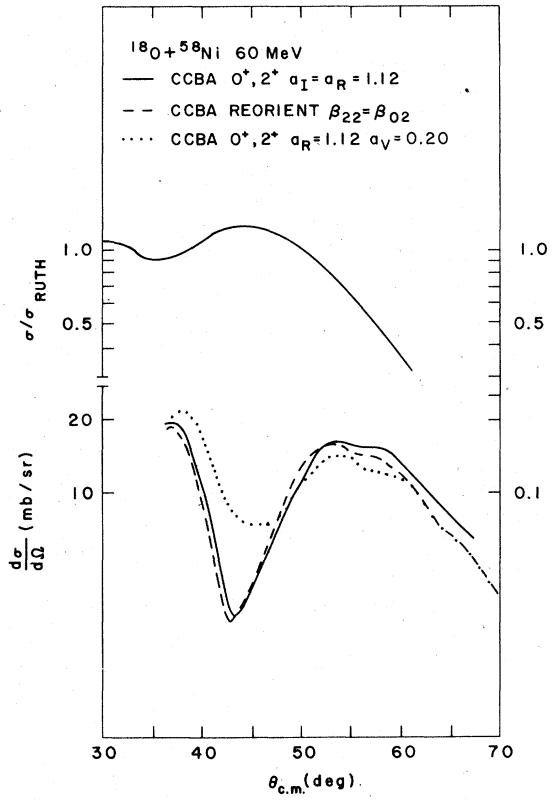

FIG. 7. Further variations in the inelastic calculations of Figs. 5 and 6. The depth of the nuclear-Coulomb dip is clearly strongly dependent on interference between imaginary and real *nuclear* terms in the form factor ($F2$ and modifications). Reorientation is carried out using a "rotational" value for the 2_1^+ quadrupole moment. Doubling the latter moment produces a linear variation in the effect, still essentially small and not enough to remove the discrepancy obtained with a purely macroscopic form factor (Fig. 5).

for the ^{58}Ni target. Slight modifications might be expected in the $^{18}O+^{60}Ni$ potentials, but to facilitate comparison of cross-section magnitudes we have eschewed these. There is still, however, a built-in $(A_1^{1/3}+A_2^{1/3})$ dependence in optical radii. Comparison between the model calculation and data for $^{18}O+^{60}Ni$ at 63 MeV are shown in Fig. 9. Again a reasonable description of the data is obtained.

In the transfer reactions one must also employ optical potentials for $^{16}O+^{60,62}Ni$ scattering. Potentials 4, 5, and 6 in Table I were used in various calculations with $P4$ and $P5$ providing reasonable fits to available Brookhaven data at 61.41 MeV for a ^{60}Ni target and at 54 MeV for a ^{62}Ni target. Com-

TABLE IV. ^{18}O wave functions obtained in the ($1s$-$0d$) shell model space with oscillator wave functions (see Ref. 23).

State	Configuration					
	$d_{5/2}^2$	$d_{5/2}s_{1/2}$	$s_{1/2}^2$	$d_{5/2}d_{3/2}$	$d_{3/2}s_{1/2}$	$d_{3/2}^2$
0_1^+(g.s.)	0.865		0.452			0.218
2_1^+	0.753	0.612		0.087	−0.211	0.084
4_1^+	0.962			0.273		
0_2^{+*}	−0.449		0.891			−0.068
2_2^+	0.650	−0.748		−0.023	0.127	−0.028

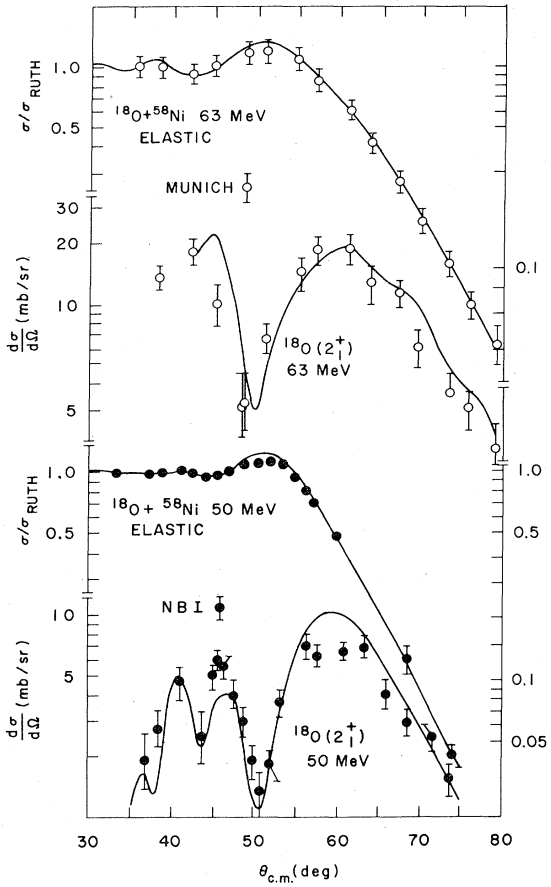

FIG. 8. Comparisons between further elastic and inelastic $^{18}O+^{58}Ni$ data and predictions of ($P3$-$F2$) CHUCK calculations. A reasonable description is obtained.

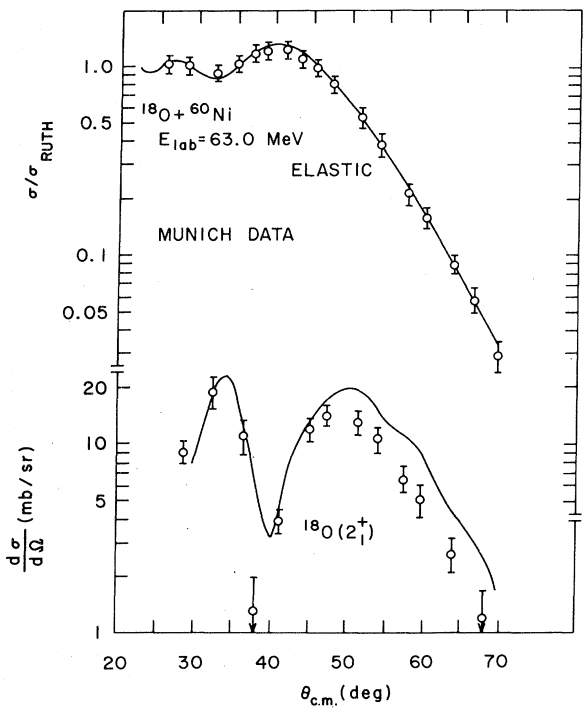

FIG. 9. Data and theory for $^{18}O+^{60}Ni$ at 63.0 MeV. No change aside from adjustments for $A_{\text{target}}^{1/3}+A_{\text{projectile}}^{1/3}$ is made in potential parameters, and apparently little change is needed.

parison between calculations using $P4$ and the data appears in Fig. 10.

The effects of target excitation were examined using the standard macroscopic prescription for the form factor. No difficulties arise from treating excitation of the rather collective Ni(2^+) states and a prediction for $^{18}O+^{58}Ni \rightarrow {}^{18}O+{}^{58}Ni(2^+)$ is shown in Fig. 11. When more than just a few valence nuclear states are involved in the transition the slower drop off of the last few nucleons is apparently not evident. Again coupling between $^{58}Ni(0_1^+)$ and $^{58}Ni(2_1^+)$ is small within our choices of potential and readjustment of elastic scattering potentials for the following transfer calculations seems unnecessary.

We conclude this section by reiterating our earlier statement that inelastic and elastic data serve

TABLE V. Spectroscopic amplitudes calculated for transfer in the cluster permitting the maximum number of nodes on the coordinate between two neutron center of mass and nuclear center. When these amplitudes are employed in MARS the signs of ($0^+ \rightarrow 2^+$) must be changed.

(^{16}O, ^{18}O)	($0_1^+ \rightarrow 0^+$)	($0_1^+ \rightarrow 2_1^+$)	($0_1^+ \rightarrow 4_1^+$)	($0_1^+ \rightarrow 2_2^+$)
	0.536	+0.504	0.413(0.500)	−0.235
(^{58}Ni, ^{60}Ni)g.s.-g.s.	0.636	0.25		
(^{60}Ni, ^{62}Ni)g.s.-g.s.	0.609	0.25		
(^{62}Ni, ^{64}Ni)g.s.-g.s.	0.615	0.25		
(^{64}Ni, ^{66}Ni)g.s.-g.s.	0.590	0.25		

mainly to fix some of the optical potential and form factor parameters entering into the coupled-channel transfer calculations. However, it is clear that these data have lives of their own. In particular the excitation of the 2_1^+ state of ^{18}O is especially sensitive to the choice of form factor. Our particular selection would seem to have eliminated a previous problem, but this point should be justified by a detailed semimicroscopic calculation. The choice of absorption parameters in the elastic potential is probably not completely determined by the elastic and inelastic data. The sensitivity of the predictions to the imaginary part of the potential is not so evident in the angular regions considered here, but perhaps will show up as more backward angles are explored. However, distinct differences from predictions made with the so-called strong absorbing or surface-transparent potentials are very clear in transfer differential cross sections.

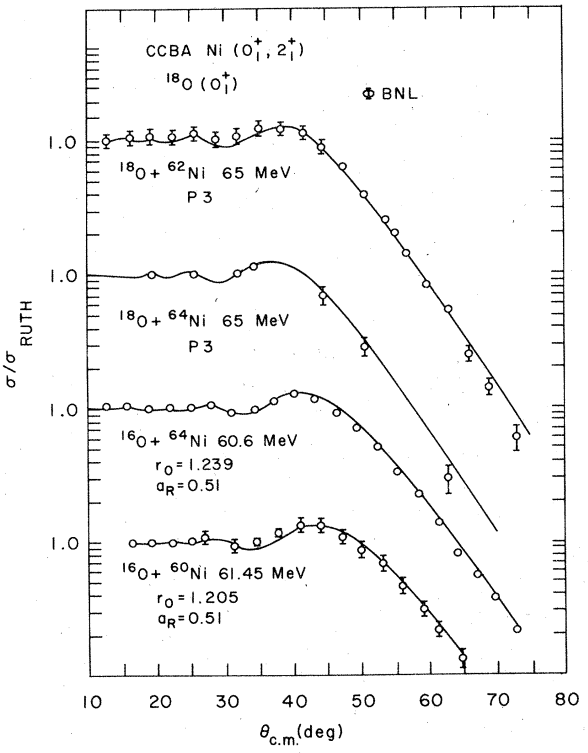

FIG. 10. Elastic predictions made with CCBA including the target 2_1+g.s. channels for ^{16}O+ ^{60,64}Ni and further ^{18}O+ ^{62,64}Ni scattering. The ^{16}O potentials to be used in the following transfer calculations are determined and the universality of the ^{18}O potential further tested. A change of ^{16}O potential is required for the heavier Ni isotopes, and a similar change may be necessary in ^{18}O+ ^{64}Ni. These changes however produce little effect on transfer (see Fig. 22).

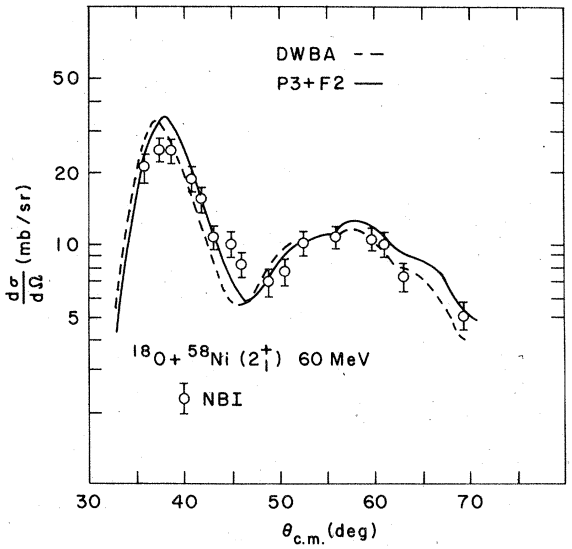

FIG. 11. Target excitation. Comparison with data for ^{58}Ni(2_1^+) inelastic excitation using a macroscopic form factor defined by $P3$ and coupling determined from the $BE(2)$ in Table II. The elastic scattering cross section is virtually unaltered by this coupling and CCBA differs only slightly from DWBA.

IV. COUPLED CHANNEL TREATMENT OF THE TWO NEUTRON TRANSFERS

A. Projectile excitation

Most of the ingredients necessary for performing a coupled-channel calculation for the (^{18}O, ^{16}O) and (^{16}O, ^{18}O) reactions have been assembled. Still required are two-particle form factors for the transfer channels considered. Before these are constructed, however, one must consider the merits of different available approximations to the reaction mechanism. In Ref. 1 a no-recoil DWBA analysis was employed. This was subsequently compared with a finite range calculation, and shown to give substantially correct angular distributions. However, the ratio in magnitude between recoil and no recoil cross sections is generally quite different from unity and dependent on energy, Q value, and L transfer. The implications for coupled-channel calculations are obvious; it would be difficult to believe the several transfer routes in a no-recoil CCBA (coupled-channel Born-approximation) calculation are properly relatively normalized. The transfer calculation in Ref. 4 is, in fact, a no-recoil approximation using a microscopic two-particle form factor. One patching procedure of some validity would use a finite range theory to correct the normalizations of all transfer routes entering into the no-recoil coupled-channel computation. We have done this

to some extent in a separate comparative, no-recoil calculation which simply checked the results of Ref. 4. For the most part, however, we have decided to rely on the full finite coupled-channel version of the codes SATURN and MARS, later presenting some finite range, microscopic, and DWBA calculations by Bayman.[20,21]

In Ref. 4 the normalization of the ^{16}O(g.s.) $\rightarrow$ ^{18}O(2^+) transfer route is accomplished by comparison with actual data, yet another attractive if *ad hoc* approach. Unfortunately the normalization appears to have been arrived at by the use of a single unrepresentative point in the data. In Fig. 2 where the Berkely data for the ^{60}Ni(^{16}O, ^{18}O(2^+))^{58}Ni(g.s.) reaction at 73.2 MeV is compared with theoretical DWBA predictions, this normalization procedure is displayed. The calculation in Ref. 4, only slightly altered after channel coupling, crosses the data at $\theta_{c.m.} = 32.6°$ where the 2^+/g.s. ratio is 3.4. An average over all measured points gives a value for this ratio closer to 2–2.5. The improved, but still simplified, theory we outline below comes close to predicting this important experimental observation.

The finite range codes SATURN and MARS are constructed for single-particle transfer and thus cannot directly utilize a microscopic two-particle transfer form factor. Our approach in constructing transfer form factors has been the standard one of selecting appropriate wave functions, for say ^{16}O, ^{18}O, and the Ni isotopes in a harmonic oscillator basis, and then expanding in a Talmi-Moshinsky[22] series to separate out two-neutron relative and center of mass coordinates. In such an expansion the dominant transfer term is obtained from placing a maximum number of nodes on the center of mass coordinates, i.e., the coordinate which defines the separation between the two-neutron cluster center of mass and the nuclear potential center. Any error in such an approach arises from the assumption, probably reasonable, that two-neutron relative coordinates change little during transfer. In any case errors from this "cluster-like" approximation to the two-particle form factor are only mildly dependent on projectile or target states, unlike the rather drastic errors of normalization in a no-recoil calculation. We have, in fact, compared the results of using the recoil cluster form factor, artifically normalized to agree with the calculation in Ref. 4, with the result of a no-recoil microscopic form factor and found quite similar angular distributions. Thus the use of microscopic form factors is unlikely to introduce any new features into the angular shapes extracted from the coupled-channel theory. In contrast the exclusion of recoil corrections may very well have serious consequences.

The wave functions for ^{18}O were constructed from purely $(sd)^2$ components,[23] and are listed in Tables IV and V. Also shown in these tables are (pfg) shell components for the (^{4}Ni, $^{A-2}$Ni) two-neutron form factors. The construction of two-particle form factors to be inserted into the reaction codes follows straightforwardly from this information. Of course, within the reaction code, the actual cluster two-neutron center of mass wave function is treated in a Woods-Saxon well, and given the appropriate separation energy. All that need be obtained from Tables IV and V then is an effective cluster-spectroscopic factor and these are listed in Tables IV and V as well. The second 0_2^+ state in ^{18}O is in general accepted as a mixed core-excited and $(sd)^2$ shell model state. In any case, one does not expect, and in, say, (t,p) reac-

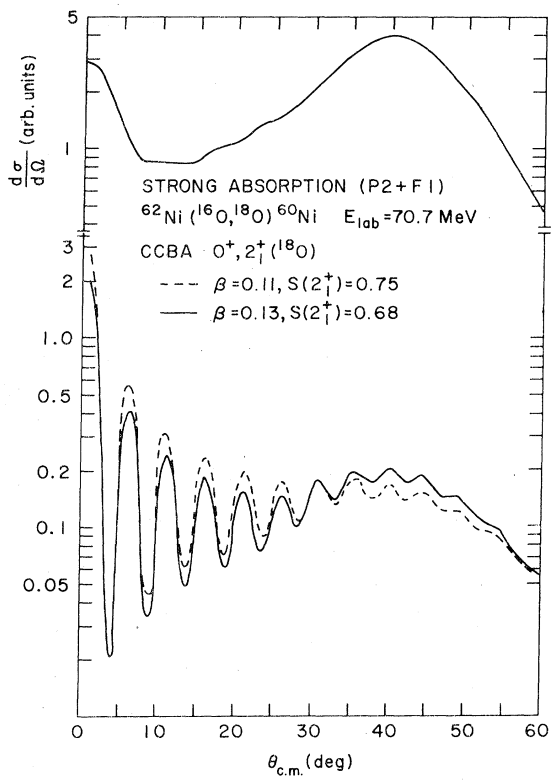

FIG. 12. Transfer from strong absorption CCBA with $(0_1^+, 2_1^+)^{18}$O channels. Some difficulty is experienced in fitting the 2^+/g.s. ratio as well as the ground-state angular distribution within the finite-range cluster framework used here. A very small ground-state cross section is predicted, perhaps an order of magnitude less than that shown in Fig. 13. The same "arbitrary units" indicated in this figure are consistently employed throughout the remaining transfer calculations, except where otherwise indicated. $P2$ and $F1$ are employed.

tions[24] does not see, strong two-particle transfer to this state. In our model calculations the effects of the 4_1^+, 2_2^+, and 0_2^+ states are separately added on to those of the 2_1^+ states already discussed in Ref. 4. Our principal disagreements with the predictions of the strong absorbing potential model arise from coupling to this later 2_1^+ state. An outstanding conclusion is that higher excited states in the ^{18}O spectrum, when reasonably normalized, do not greatly affect transfer, nor as we have already seen inelastic, angular distributions.

Anticipating this result that coupling to the second group of excited states in ^{18}O, i.e., to $4_1^+, 0_2^+$, 2_2^+, only slightly alters the transfer cross sections in angular shape or magnitude we use as a standard calculation one involving coupling only between the ^{18}O ground and 2_1^+ states. The ^{16}O projectile is assumed unexcited and coupling to Ni states in entrance or exit channels is treated later. Thus in Fig. 12, CCBA calculations are displayed for the selection, potential $P2$ (Table I) and form factor $F1$ (Table II), i.e., for the strong absorbing choice. The transfer spectroscopic strengths used for this calculation are 0.536 for the ^{16}O 0^+ to 0^+ transition and 0.68 to 0.75 for 0^+ to 2^+. The latter strength has been adjusted to parallel the choice in Ref. 4 and to produce a realistic angular distribution for the ground-ground state (^{60}Ni, ^{62}Ni) transfer. The g.s. transition is compared with data exist from the Lawrence Berkeley Laboratory.[8] ition to ^{16}O+^{60}Ni for which at least preliminary data exist from the Lawrence Berkely Laboratory.[8]

The calculations employing $P3$, $P4$, and $F2$ and spectroscopic factors (0.536, 0.504), i.e., with surface transparent potentials, are displayed against available data in Fig. 13. In the latter figure the ^{60}Ni(^{18}O, ^{16}O)^{62}Ni ground-state transition is normalized to data and the other calculations normalized as indicated. Absolute cross-section magnitudes will be discussed in the next section in detail, but for the moment we note Figs. 12 and 13 suggest the ground-state transitions are an order of magnitude stronger for the surface absorbing potentials.

Selected comparisons between $(0^+, 2^+)$ coupling and pure DWBA are shown in Fig. 14; DWBA here is not represented by the so-called direct term discussed elsewhere[4,9] but obtained by truly switching off coupling. The coupling is, of course, a very large effect for the ground-ground state transition in the presence of strong absorption, rendering a smooth bell-shaped distribution forward rising and oscillatory. In the framework favored here coupling is much less important, a situation to be preferred if one views DWBA as the first term in a perturbative series. We emphasize that the degree of coupling is both optical potential and form factor dependent. If in our extended form factor $F2$ only the real part is given the larger diffusivity $a_R = 1.12$ fm then $(0^+, 2^+)$ coupling differs from DWBA by up to factors of 2

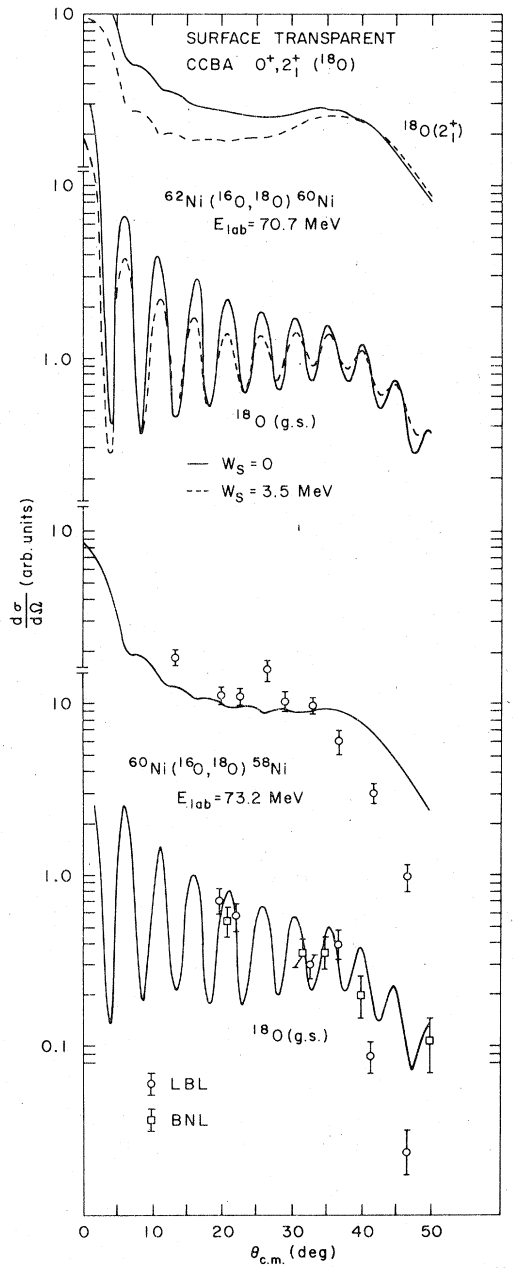

FIG. 13. Surface transparent CCBA with $(0_1^+, 2_1^+)^{18}$O channels for two neutron transfer in ^{16}O incident on $^{60, 62}$Ni targets. Comparison is made to data for the ^{60}Ni target and especially to be noted is the contrast between Figs. 12 and 13 for the ^{18}O(2_1^+) excitation. Absolute normalization of theory is discussed later. The theoretical calculations are, however, correctly relatively normalized and given in the same units as in Fig. 12. $P3$, $P4$, and $F2$ are used.

(Fig. 14), a much larger effect than with $a_I = 1.12$ fm as well. Apparently producing the deep minimum in the inelastic excitation of $^{18}O(2^+)$ by ^{58}Ni leads to a reduction in the effect of channel coupling in transfer.

The $(0^+, 2^+)$ coupling model presented in Figs. 12–14 includes, of course, Coulomb excitation treated in the fashion discussed in Sec. II. To illustrate the importance of Coulomb excitation in transfer calculations, this term in the inelastic $0_1^+ \to 2_1^+$ form factor is switched off and the results plotted in Fig. 14 for the $^{60}Ni(^{16}O, ^{18}O)\ ^{58}Ni$ reaction at 73.2 MeV, i.e., at the equivalent of 65 MeV for ^{18}O ions in the inverse reaction. In the g.s.-g.s. transition changes $\lesssim 25\%$ are seen; virtually no change occurs omitting Coulomb excitation when the $^{18}O(2_1^+)$ state is excited in transfer. In the present situation one may conclude including Coulomb excitation slightly decreases the effective channel coupling.

Excitation of the "two phonon" states of ^{18}O be-

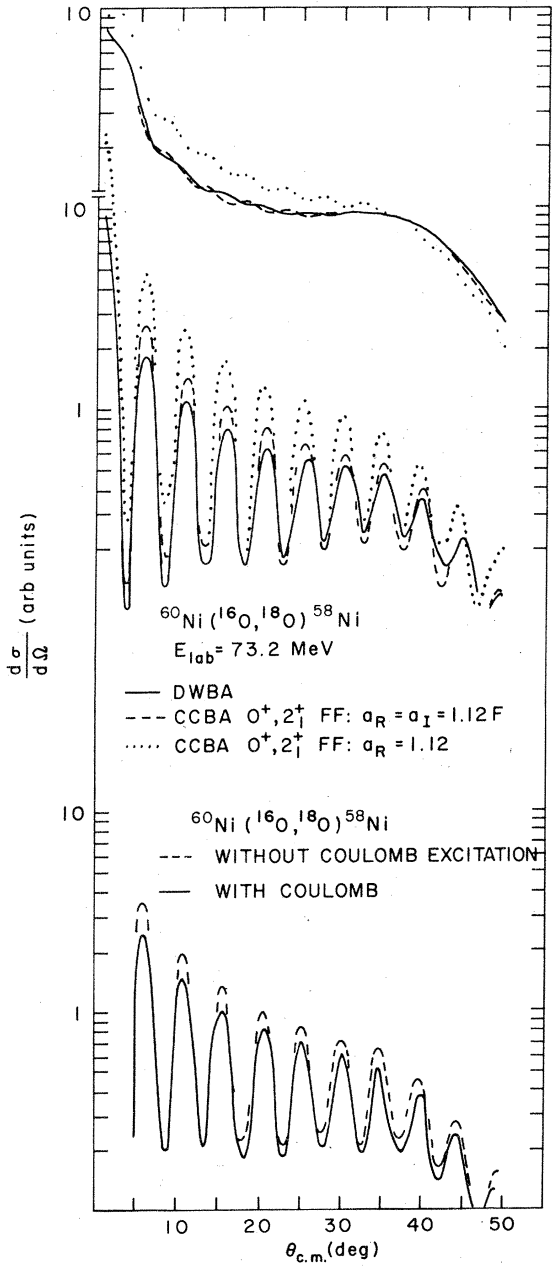

FIG. 14. Further CCBA with surface transparent potentials ($P3, P4$) but variations in the form factor. First a comparison is made to the result in Fig. 13 and to DWBA for ^{18}O(g.s., 2_1^+) excitation obtained with only an extended real part in the form factor. Clearly the nuclear real-imaginary interference evident in the inelastic 2_1^+ excitation reduces the effect of coupling. Secondly, the effect on the CCBA of omitting Coulomb excitation in the form factor is shown.

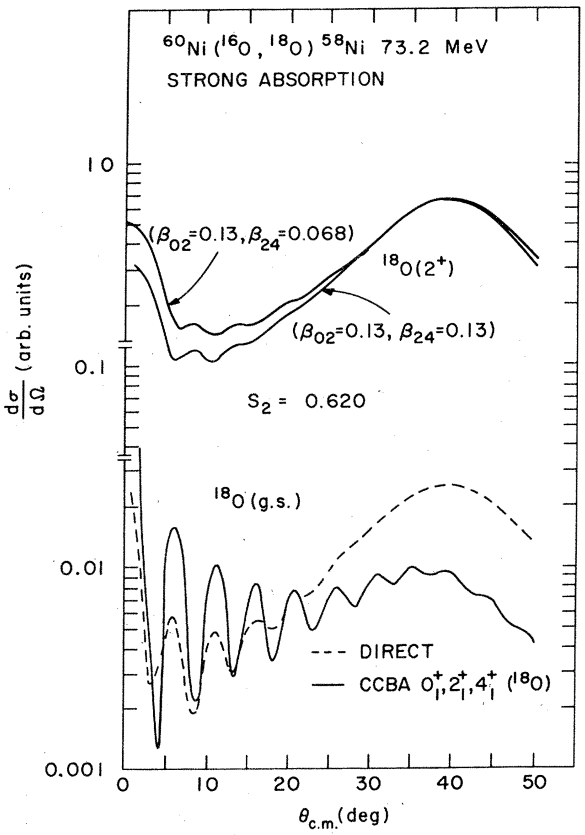

FIG. 15. Transfer in CCBA for strong absorption ($P2+F1$) with $^{18}O(0_1^+, 2_1^+, 4_1^+)$ coupling. The $2_1^+ \to 4_1^+$ form factor is identical to that for $0_1^+ \to 2_1^+$; the couplings used are as demanded by the $BE(2)$ $2_1^+ \to 4_1^+$, and also twice this value. Coulomb excitation is omitted from $F2$, but would not significantly alter the conclusion that the 4_1^+ channel is a small perturbation. The alternate coupling scheme 0_1^+, 2_1^+, 2_2^+ produces similar results and simultaneous inclusion of 2_2^+, 4_1^+ seems unlikely to be important.

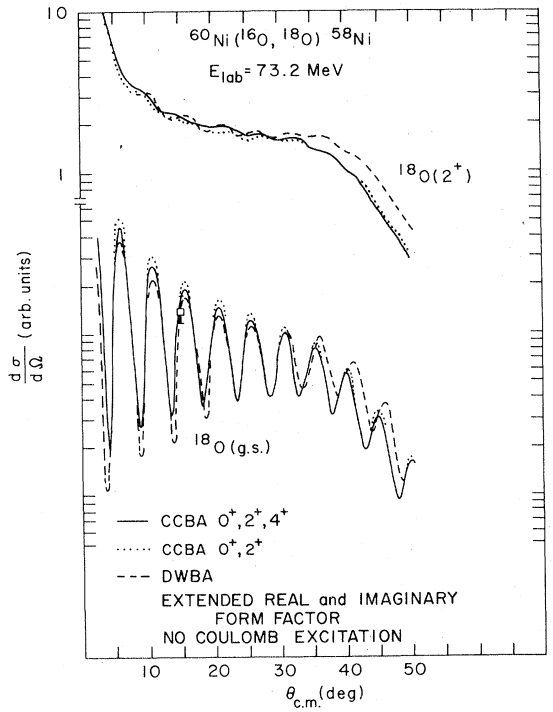

FIG. 16. Two neutron transfer in CCBA with 0^+_1, 2^+_1, 4^+_1 coupling and surface transparent potentials ($P3$,$P6$). Again Coulomb excitation is not included in the form factor. This latter omission and the altered ^{16}O potential do not greatly affect the results. Coupling to 2^+_2 is also a small effect.

tween 3.55 and 3.92 MeV was handled sequentially, each of the states being introduced into the model separately. The coupling strengths used are described in Table II and the spectroscopic strengths in Table IV and V. Variations in the one- to two-"phonon" coupling strength were made, to increase these as much as a factor of 2 above reasonable values; yet in all cases considered this higher group of states played little role in the transfer cross sections. This conclusion is especially important for the strong absorbing calculation. The authors of Ref. 4 had been hopeful that inclusion of such coupling would remedy their failure to fit the angular distribution for transfer to ^{18}O(2$^+$). The results of a $0^+_1, 2^+_1, 4^+_1$ coupling scheme are shown in Fig. 15, and it is apparent little change occurs. Similar results obtained for 0^+_1-2^+_1-2^+_2 and 0^+_1-2^+_1-0^+_2. Part of the difficulty in altering the important ^{16}O(0$^+$) → ^{18}O(2$^+$) differential cross section follows from the large interference between one- and two-step routes introduced to produce the desired ground-ground angular distribution. This interference was obtained from an overly large spectroscopic normalization of the 0$^+$ → 2$^+$ transfer route, yielding stability against further coupling in the predicted 2$^+$ distribution.

Even so, when reasonable spectroscopy is selected together with $P3$, $P6$, and $F2$ coupling to 4^+_1, 2^+_1, or 0^+_2 seems unimportant, as is evident in Fig. 16. The calculation in this case was performed leaving Coulomb excitation out of the inelastic form factor and thus likely includes an *enhancement* of the channel coupling. Little difference can be expected with Coulomb terms retained.

B. Target excitation

The authors of Ref. 4 have stated that target excitation is unimportant for reactions considered

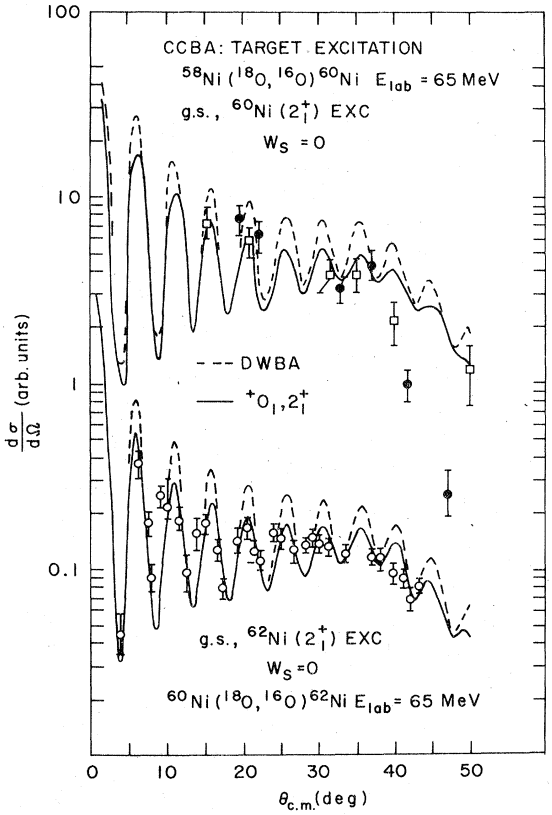

FIG. 17. Transfer in CCBA with target excitation. The residual nuclear 2^+_1 ^{60,62}Ni channels are included. Coupling to the initial target 2^+_1 state might be expected to interfere destructively (Ref. 26) but is reduced in strength by Q dependence. Calculations allowing 2^+_1 (initial target) → 2^+_1 (residual nucleus) transfer were made and indicate small but not negligible effects which should be further studied. The CCBA target excitation seems to produce a larger effect on magnitudes than did projectile excitation. The (^{60}Ni, ^{62}Ni) data have been normalized to place it relative to the theory and the (^{58}Ni, ^{60}Ni) data then relatively reduced by ~15%. Absolute normalization is discussed later. Macroscopic form factors used were obtained from $P4$, $P5$ and couplings obtained from Table II.

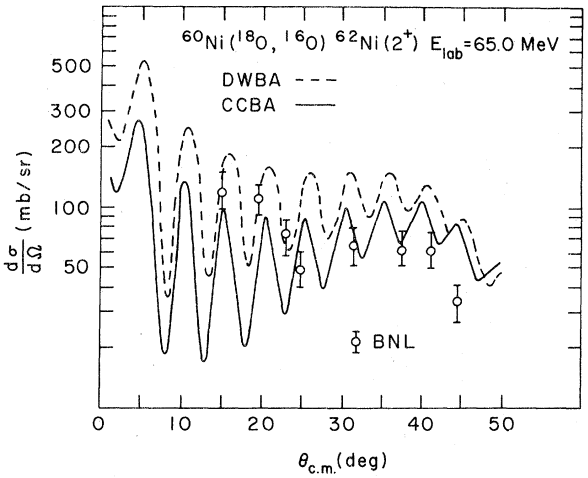

FIG. 18. Target excitation in CCBA transfer. Differential cross sections for ^{62}Ni(2$^+$) excitation obtained with the scheme discussed in Fig. 17. No renormalization relative to the ^{60}Ni(^{18}O, ^{16}O) g.s. cross section in Fig. 17 has been performed, but the (^{60}Ni, ^{62}Ni), 2$^+$ spectroscopic factor used is larger than predicted by theory. Again the initial target -2_1^+ coupling is less important but further study is required here.

here. This appears true in the strong absorption model using $P2$ and $F1$. However, with the surface, transparent potentials, apparently necessary to fit the angular distribution in the (^{16}O, ^{18}O(2_1^+)) reaction, target (or residual target) excitation has an appreciable effect on magnitudes of ground-ground state transitions. In Fig. 17 we display the CCBA and DWBA predictions for the reaction

$$^{18}\mathrm{O} + {}^{58}\mathrm{Ni} \rightarrow {}^{16}\mathrm{O} + {}^{60}\mathrm{Ni(g.s.)}.$$

The Ni(0$^+ \rightarrow$ 2$^+$) coupling strengths are matched to known electromagnetic transition amplitudes[7,25] and the spectroscopy for transfer adjusted to produce correct normalization for the ^{60}Ni(2$^+$) state relative to ground state (see Table II). Relative to DWBA the CCBA angular distribution is somewhat flattened at forward angles and for angles backward of 20° magnitude changes of up to 35% occur. Simultaneous excitation of the ^{58}Ni(2$^+$) state does not alter these results significantly. One expects[26] destructive interference between the transfer routes A, ^{58}Ni(2$^+$) $\rightarrow$ ^{60}Ni(g.s.) and B, ^{58}Ni(g.s.) $\rightarrow$ ^{60}Ni(2$^+$), but the larger separation energy, S_A = 21.83 MeV vs S_B = 19.05 MeV suppresses the ^{58}Ni excitation. In Fig. 18 we display predicted angular distributions for the (^{58}Ni, ^{60}Ni(2$^+$)) differential cross section at 65 MeV, including target excitation during transfer. Our choice of spectroscopic factors for 0$^+ \rightarrow$ 2$^+$ transfer is dictated by the experimental data[1] for excitation of ^{60}Ni(2$^+$). Clearly the angular distribution for this latter state is sensitive to both the reaction mechanism and the spectroscopy of the Ni isotopes. A careful study of these states should be pursued, but will not greatly alter the major conclusion of the preceding sections of the present work on excitation of the ^{18}O(2_1^+) state in the (^{16}O, ^{18}O) reactions.

V. FURTHER PARAMETER VARIATION AND CROSS-SECTION MAGNITUDES

A. Parameter Variation

It is instructive to vary the degree of absorption within the surface transparent approach. One can thereby demonstrate that the absorption does play a role in angular shapes. In Ref. 5 the absorption is discussed in detail and consists of two pieces

$$W(r) = W_V(r) + W_S(r), \tag{13}$$

$$W_V(r) = -W_0^V f(x_V), \tag{14}$$

$$W_S(r) = 4W_0^S f'(x_S), \tag{15}$$

with

$$f(x) = [1 + \exp x]^{-1} \tag{16}$$

and

$$x_{V,S} = \frac{r - R_{V,S}}{a_{V,S}}. \tag{17}$$

The surface transparency is achieved by taking a small volume diffusivity $a_V \approx 0.2$ to 0.3 and a small surface depth $W_0^S \approx$ few MeV. We do not expect ion-ion potentials to be surface transparent in all situations. Valence nucleon configurations and energy variation will have obvious effects. A simple and probably physical way[5] to allow for varying surface absorption is to permit W_S to change. Thus in Fig. 19 we have calculated the g.s. and ^{18}O(2_1^+) coupled-channel angular distribution as a function of W_S. A sufficient increase in W_S converts this transfer angular shape into that obtained from the strong absorption choice, but has a barely noticeable effect on elastic and inelastic predictions. The cross-section magnitude (at peaks in oscillatory distributions) is also clearly reduced by an increase in W_S.

In the CCBA surface-transparent calculations performed in the last section we used $0 \leq W_S \leq 3.5$ MeV, with the smaller value of W_S probably preferred for ^{16}O + ^{60}Ni and the upper value perhaps better for ^{16}O + ^{62}Ni. The shapes of ^{16}O(g.s.)-^{18}O-(2$^+$) and the ^{16}O(g.s.)-^{18}O(g.s.) angular distributions determine this preference, which is then reflected somewhat in relative magnitudes of cross sections for the two targets.

Variations in the diffusivity a_V and strength W_V of the volume absorption are also shown in Figs. 19 and 20, thus completing the excursion from

surface transparent to strong absorbing potentials. The extreme cases included are certainly distinctively different in shape, but some intermediate choices of volume absorptive parameter might very well work as well.

One can equally well perturb the angular distributions by alterations in real parameters. As an example we may use $P5$ in place of $P4$, i.e., alter the ^{16}O optical potentials but not the fit to available ^{16}O elastic scattering, and somewhat alter angular distributions. No great significance should be attached therefore to the larger real and imaginary diffusivities in the ^{16}O potential $P4$ relative to $P3$. More violent changes in real parameters, for example, increasing the real diffusivity to >0.5 fm in $P4$, tend to drive the g.s. angular distribution towards bell-shaped, though the absorptive potential remains surface transparent. Our original caveat, in Sec. II, that a surface-transparent potential be judged by its ground-ground DWBA prediction must be heeded.

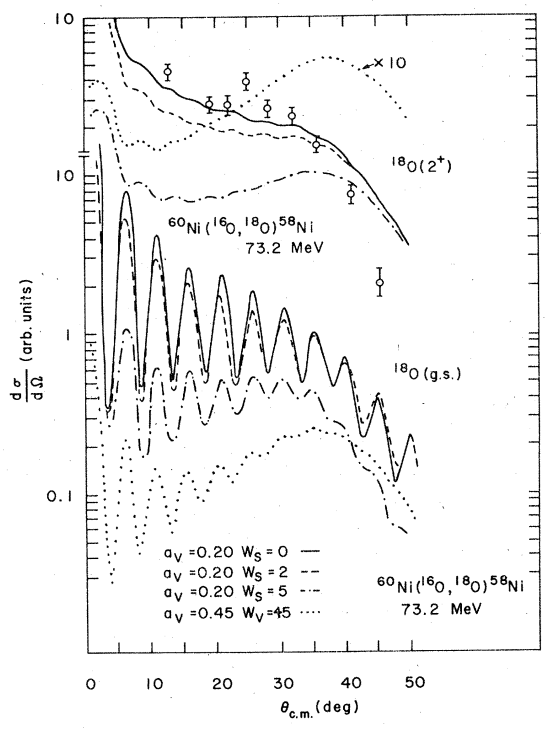

FIG. 19. Variations in CCBA transfer calculations due to alterations in the optical potentials. Changes in the surface absorption W_S and finally in the volume diffusivity a_V and volume absorption W_V produce a smooth transition from surface transparency to strong absorption. The calculations are made using ($P3$,$P6$) and no Coulomb excitation in the form factor, but the general trend is independent of these details.

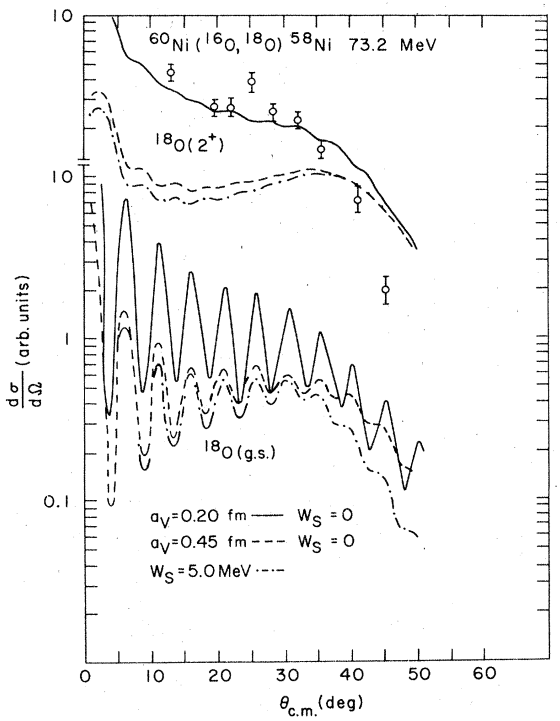

FIG. 20. Further variations in the potential parameters a_V and W_S.

B. Magnitudes

One aspect of two-particle transfer which is certainly inadequately handled in all existing theories of the reaction mechanism is the absolute size of such cross sections. This problem applies to the theory of light-ion as well as heavy-ion induced transfer. No systematic study of cross-section magnitudes obtained in the presence of channel coupling has been performed. Some authors[27,28] have suggested successive transfer of the two nucleons provides a substantial correction to cross-section magnitudes if not to angular distributions. It has not been our primary purpose here to consider absolute magnitudes but it is of some interest to examine the results of our calculations in this regard and of course imperative to consider relative magnitudes. We have already noted the strong absorbing potentials can lead to consistently smaller cross-section magnitudes. In the (^{18}O, ^{16}O) ground-state transitions a destructive interference between direct and indirect routes reduces the cross section at grazing angles by an order of magnitude. For surface transparent potentials the interference is some times constructive, sometimes destructive, but never a dominant effect.

In fact, although we did not emphasize this in

TABLE VI. Relative magnitudes in ^{60,62}Ni(^{16}O,^{18}O)^{58,60}Ni at E_{lab}=73.2, 70.7 MeV. These results are taken from Figs. 13 and 17. The spectroscopy is from Table IV and V.

$\theta_{c.m.}$	$\theta_{c.m.}$	19.6°	22.2°	32.6°	36.4°	41°
^{58}Ni-^{18}O(2$^+$)/^{18}O(g.s.)	Theory	1.7	2.5	3.2	2.0	3.2
	Expt.	1.7	2.1	3.4	1.8	2.7
	$\theta_{c.m.}$	15°	32°	37°	40°	
$(60,58)_{g.s.}/(62,60)_{g.s.}$	Theory	3.0	3.8	2.7	3.1	
	Expt.	2.7	3.6	2.7	4.45	

Secs. III and IV, it is difficult *when using strong absorbing potentials* within the cluster finite range computations to reproduce both the ground-ground state shape and the 2$^+$/g.s. relative cross section in the ^{60}Ni(^{16}O,^{18}O)^{58}Ni reaction at E_{lab}=73.2 MeV. The degree of destructive interference required to reproduce the ground-state shape leads to a magnitude reduced by more than an order of magnitude from the DWBA, whereas the 2$^+$ cross section is only slightly affected by channel coupling.

Relative cross-section magnitudes are remarkably well reproduced by our standard calculation ($P3,P4,F2$). The spectroscopy employed in this calculation emerged from a typical ($1s$-$0d$) shell model calculation.[23] The predictions for relative magnitudes are summarized in Table VI; both the 2$^+$/g.s. ratio for the ^{60}Ni target in the (^{16}O,^{18}O) reaction and the g.s. to g.s. ratio for ^{58}Ni/^{60}Ni targets are rather well described. Calculation also indicates that relative predictions for ^{62,64}Ni targets are reasonable. (See Fig. 22.) A slight tuning in g.s. to g.s. ratios among the Ni isotopes will occur from changes in surface absorption strength (W_S) made, if necessary, to reproduce angular shapes. More detailed data are needed, before this can be accomplished with confidence.

Absolute magnitudes may also be considered within the present framework, though perhaps with less validity. Some corrections to our magnitude predictions can be expected from the cluster approximation used in the finite range form factor and also from the indirect terms here omitted but required to produce post-prior equality. Predictions follow from Tables IV and V by extracting the (^{58}Ni,^{60}Ni) spectroscopic factor. One finds with the wave functions used previously in Ref. 1 and extracted from an early pairing calculation of Kisslinger and Sorensen[29]

$$S(^{58}\mathrm{Ni},^{60}\mathrm{Ni})_{g.s.}=0.636 \tag{18}$$

and thus for example

$$\frac{d\sigma}{d\Omega}\,(\theta_{c.m.}=21°)=17\ \mu\mathrm{b} \tag{19}$$

for the ^{58}Ni(^{18}O,^{16}O)^{60}Ni reaction at 65 MeV. Here we include the effects of target excitation which reduce overall cross-section magnitudes. The experimental value lies in the range 50±5 μb. The cluster, finite range calculation thus underpredicts the two-neutron transfers by approximately a factor of 3.0. Since the DWBA (Figs. 1 and 2) quantitatively reproduces the present CCBA model, one may appeal to an exact finite-range microscopic estimate of the magnitude. Bayman has kindly performed such a calculation for us and we quote his results.[20]

In Fig. 21 are displayed comparisons between DWBA calculations, in the post version, calculated in the cluster approximation using the codes MARS-SATURN or LOLA,[30] and also calculated using the microscopic finite range code. The agreement in angular distribution between the cluster microscopic codes is remarkable. Even more remarkable perhaps is the agreement in magnitude between microscopic and cluster calculations, which employed the same spectroscopy for (^{18}O,^{16}O) and (^{58}Ni,^{60}Ni) overlaps. For example, at the angle referred to in Eq. (19)

$$\frac{d\sigma}{d\Omega_B}^{\mathrm{DWBA,\,cluster}}=24.2\ \mu\mathrm{b}, \tag{20}$$

$$\frac{d\sigma}{d\Omega}^{\mathrm{DWBA,\,microscopic}}=18\ \mu\mathrm{b}. \tag{21}$$

One might then expect perhaps a 25% decrease from magnitudes predicted by the cluster calculation, and in fact finds a similar factor for (^{18}O,^{16}O) reactions on both ^{58,60}Ni targets (see Fig. 21).

One further point which has been checked in the present work is agreement between post and prior versions of DWBA. The agreement between the cluster calculations obtained between MARS-SATURN and LOLA persists, but not quite so well, in the prior representation. However, prior cross sections are close to twice the size of post; nor does inclusion of the so-called Coulomb indirect terms[31] remove this discrepancy. Since the post repre-

sentation of the reaction ^{58}Ni(^{18}O, ^{16}O)^{60}Ni involves the smaller projectile size in the form factor, one expects the indirect terms, nuclear or Coulomb, to change it less.

We are left with the conclusion that the computation of absolute cross-section magnitudes in heavy-ion two-particle transfer is strongly optical potential dependent. The present calculation underpredicts experimental differential cross sections by considerably less than earlier work.[21] In Figs. (20) and (21) we have used optical potentials with no surface absorption; increasing W_S to, say, 3.5 MeV for both ^{18}O and ^{16}O potentials in (^{58}Ni, ^{60}Ni) decreases magnitudes by some 20%.

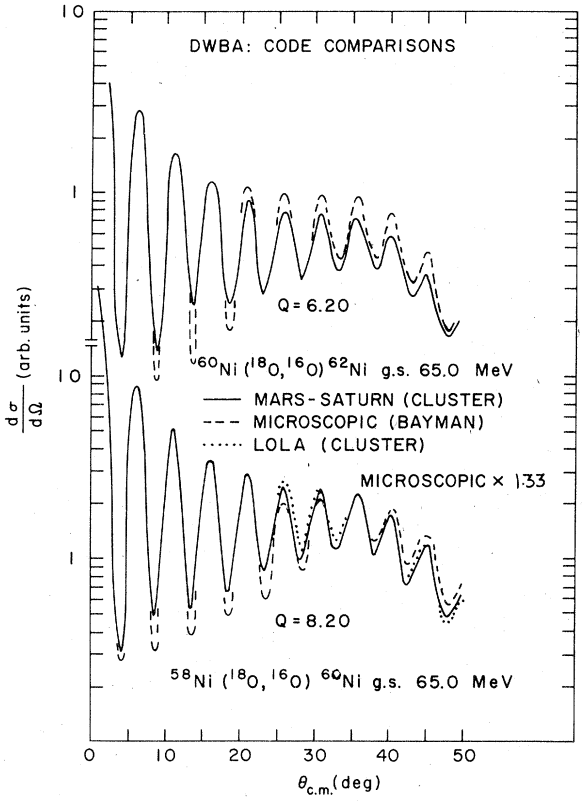

FIG. 21. Comparisons between cluster and microscopic DWBA calculations for ground-state transitions. The cluster calculations with MARS-SATURN and LOLA are virtually identical in the post representation employed here. The slight differences appearing at angles $\gtrsim 30°$ presumably can be taken as theoretical uncertainties. The agreement in shape between the microscopic calculation by B. F. Bayman and the cluster calculation is reassuring. The close agreement in microscopic and cluster magnitude is remarkable considering the nature of the calculations. A ratio $d\sigma_{cl}/d\sigma_{mic} \sim 1.33$ is found. This ratio is nearly constant for the two target isotopes ^{60,62}Ni, despite the factor of 3–4 cross-section ratio occasioned by a strong Q dependence.

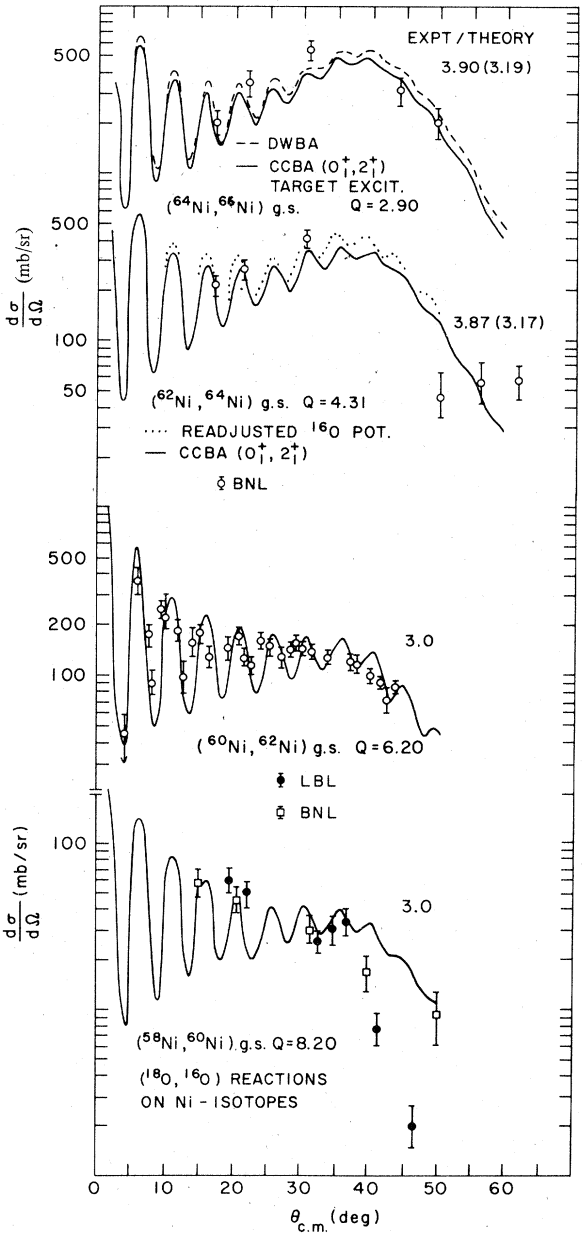

FIG. 22. A final confrontation between theory and experiment for ground-ground transitions in (^{18}O, ^{16}O) reactions on the four isotopes $^{58, 60, 62, 64}$Ni. Absolute normalization factors between theory and experiment are given and are encouragingly constant. The spectroscopic information was extracted from Tables IV and V. CCBA calculations with residual target (2^+_1) excitation were used. Universal ^{18}O and ^{16}O potentials (^{18}O, ^{16}O) were employed, but variations due to elastic constraints (indicated) change the angular distributions only slightly and yield a more constant expt./theory ratio of close to 3.0. A surface absorption $W_S = 0$ is used for $^{58, 60}$Ni targets and $W_S = 6.5$ MeV for $^{62, 64}$Ni. For the latter some surface absorption seems necessary to reproduce existing experimental shapes but $W_S = 4.0$ to 6.5 are little different.

Confidence in magnitude calculation can come, however, only by systematic study of several nuclei with the same two-nucleon transfer reaction, and from study of other similar reactions, e.g., two proton transfer. Finally then, in Fig. 22 we present the relative differential cross sections for the (^{18}O, ^{16}O) reactions on ^{58,60,62,64}Ni targets calculated using (0^+, 2^+) coupling of the residual target. Again we point out that the microscopic DWBA calculations closely agree with cluster in the (^{58}Ni, ^{60}Ni) to (^{60}Ni, ^{62}Ni) relative magnitudes. The constancy of ratio between theory and experiment, indicated in Fig. 22, is presumably a good feature of the present model.

VI. SUMMARY AND CONCLUSIONS

The rather lengthy coupled-channel calculations performed here have carefully, though perhaps not yet exhausitively, examined what may be viewed as a reasonably complete set of quasielastic data for the oxygen + nickel heavy-ion system. One began with the feeling projectile excitation was most important but ends with the likelihood target excitation plays a bigger role and should be further investigated. However, the target excitations do not seem likely to drastically change angular distributions of g.s.-g.s. or g.s.-^{18}O(2_1^+) reactions. One must certainly conclude that CCBA results are strongly potential and form-factor dependent. It is preferable therefore to select a family of potentials which minimize the perturbation due to multistep processes. It is strongly indicated that state-independent effects observed in quasielastic data should be described by the choice of optical potential. Both diffractive angular shapes and cross-section magnitudes speak to the validity of the so-called surface-transparent potentials at least for the "intermediate" projectile energies discussed here. One expects that at even lower energies, or for larger target-projectile charge products, Coulomb repulsion will make the reaction less sensitive to the absorption. At high energies, as more direct channels open, it seems likely the surface absorption strength will increase, narrowing the present distinction between surface transparent and normal potentials.

It does not follow that coupled-channel effects will always be small. Indeed it seems target excitation may be qualitatively important in this work. Transitions impeded spectroscopically or by some selection rule, as for example in the $L = 1$ spin-suppressed reactions discussed elsewhere[32,33] are a likely ground for application of CCBA. Also transitions in strongly collective, rotational bands exhibit multistep effects.[34] However, the present calculations indicate one must proceed with care. The strong CCBA perturbations seen in vibrational nuclei[9] are perhaps enhanced at low projectile energy because nuclear effects in the form factor are suppressed. The deep minimum in the ^{18}O(2^+) inelastic cross section (Fig. 5) is a signal of cancelation in CCBA effects in transfer (Fig. 14). More systematic work must be done on CCBA calculations with varying projectile energy. The global treatment of the Ni isotopes contained in Fig. 22 indicates that our quasielastic approach has some universal validity in this region.

Finally, our calculations included only a small group of excited ^{18}O and Ni states. It is possible including a very large number of coupled projectile (or target) channels would alter the angular distributions of low lying states, but we then suggest this channel coupling would best be incorporated into the optical potential when possible.

ACKNOWLEDGMENTS

We are indebted to P. D. Kunz, T. Tamura, and T. Udagawa for so selflessly providing us with their CCBA programs, and with great help in making these operational at Brookhaven. We are extremely grateful to D. Scott for sending us the very crucial LBL (^{16}O, ^{18}O(2_1^+)) data[8] prior to publication. We also wish to thank B. F. Bayman for the microscopic two-particle calculations presented here, all of which he performed for us, and also E. H. Auerbach for many useful discussions.

---

*Work supported by Energy Research and Development Administratin under Contract No. EY-76-C-02-0016.

[1]E. H. Auerbach, A. J. Baltz, P. D. Bond, C. Chasman, J. D. Garrett, K. W. Jones, S. Kahana, M. J. LeVine, M. Schneider, A. Z. Schwarzschild, and C. E. Thorn, Phys. Rev. Lett. 30, 1078 (1973).

[2]M. J. LeVine, A. J. Baltz, P. D. Bond, J. D. Garrett, S. Kahana, and C. E. Thorn, Phys. Rev. C 10, 1602 (1974).

[3]A. J. Baltz, P. D. Bond, J. D. Garrett, and S. Kahana, Phys. Rev. C 12, 136 (1975).

[4]N. K. Glendenning and G. Wolschin, Phys. Rev. Lett. 36, 1532 (1976); Nucl. Phys. A281, 486 (1977).

[5]S. Kahana and A. J. Baltz, *Advances in Nuclear Physics*, edited by M. Baranger and E. Vogt (Plenum, New York, 1977), Vol. 9.

[6]F. Videbaek, P. R. Christensen, Ole Hansen, and K. Ulbank, Nucl. Phys. (to be published); R. A. Broglia, in *Proceedings of International Conference on Reactions Between Complex Nuclei*, Nashville, North-Holland, Amsterdam, 1974), Vol. 1, p. 303 and references therein.

[7]K. E. Rehm, H. J. Körner, M. Richter, H. P. Rother, J. P. Schiffer, and H. Spieler, Phys. Rev. C 12, 1945

(1976).
[8]D. L. Hendrie, U. Jahnke, C. R. Maguire, J. Mahoney, and D. K. Scott (private communication).
[9]T. Tamura, Rev. Mod. Phys. 37, 679 (1965); T. Tamura, K. S. Low, and T. Udagawa, Phys. Lett. 51B, 116 (1974).
[10]P. D. Kunz, CHUCK, University of Colorado coupled-channels zero-range code (unpublished).
[11]A. J. Baltz and S. Kahana, Phys. Rev. Lett. 29, 1267 (1972).
[12]A. J. Baltz and S. Kahana, Phys. Rev. C 9, 2243 (1974).
[13]A. J. Baltz, Phys. Rev. C 13, 668 (1976).
[14]J. Barrette, P. Braun-Munzinger, T. Cormier, J. Harris, and M. J. LeVine, Bull. Am. Phys. Soc. 22, 563 (1977); Phys. Rev. Lett. (to be published).
[15]N. Austern, *Direct Nuclear Reaction Theories* (Wiley, New York, 1970).
[16]F. Videbaek, Ph.D. thesis (unpublished).
[17]J. L. C. Ford, K. S. Toth, D. C. Hensley, R. M. Graedke, D. J. Riley, and S. T. Thornton, Phys. Rev. C 8, 1972 (1973).
[18]H. P. Rother, Ph.D. thesis (unpublished).
[19]J. W. Olness, E. K. Warburton, and J. A. Becker, Phys. Rev. C 7, 2239 (1972).
[20]B. F. Bayman (private communication).
[21]B. F. Bayman, Phys. Rev. Lett. 32, 71 (1974).
[22]I. Talmi, in *Proceedings of the Rehovoth Conference on Nuclear Structure* (North-Holland, Amsterdam, 1958), p. 31; T. A. Brody and M. Moshinsky, *Tables of Transformation Brackets* (Monografics del Instituto de Fisica, Mexico, 1960).
[23]S. Kahana and E. Tomusiak, Nucl. Phys. 71, 402 (1965). The sign of the $(d_{3/2}s_{1/2})2_1^+$ component should be negative, and is in Table IV.
[24]R. Middleton and D. J. Pullen, Nucl. Phys. 51, 63 (1964); R. Moreh and T. Daniels, *ibid.* 74, 403 (1965).
[25]P. H. Stelson and F. K. McGowan, Nucl. Phys. A32, 652 (1962), P. M. Lesser, D. Cline, and J. D. Purvis, *ibid.* A151, 257 (1970).
[26]R. J. Ascuitto, J. S. Vaagen, and N. K. Glendenning, in *Proceedings of the International Conference on Reactions Between Complex Nuclei, Nashville* (see Ref. 6, Vol. 1., pp. 257, 137.
[27]D. H. Feng, T. Tamura, and T. Udagawa, Bull. Am. Phys. Soc. 20, 547 (1975).
[28]R. A. Broglia, U. Götz, M. Ichimura, J. Kammuri, and A. Winther, Phys. Lett. 45B, 23 (1973).
[29]L. S. Kisslinger and R. A. Sorensen, Kgl. Dan. Vidensk. Selsk. Mat.-Fys. Medd. 32, No. 9 (1960).
[30]R. M. DeVries and K. I. Kubo, Phys. Rev. Lett. 30, 325 (1973).
[31]R. M. DeVries, G. R. Satchler, and J. G. Cramer, Phys. Rev. Lett. 32, 1377 (1974); W. Tobocman, R. Ryan, A. J. Baltz, and S. H. Kahana, Nucl. Phys. A205, 193 (1973).
[32]P. D. Bond, J. D. Garrett, O. Hansen, S. Kahana, M. J. LeVine, and A. Z. Schwarzschild, in *Proceedings of the International Conference on Reactions Between Complex Nuclei, Nashville* (see Ref. 6), Vol. I, p. 55.
[33]D. Sinclair, B. Chait, S. Kahana, and B. Nilsson, Phys. Rev. C 14, 1033 (1976).
[34]K. A. Erb, D. L. Hanson, R. J. Ascuitto, B. Sorensen, J. S. Vaagen, and J. J. Kolata, Phys. Rev. Lett. 33, 1102 (1974).